A NUCLEAR MAGNETIC RESONANCE PROTON MAGNETOMETER

by

ELMER HIROSHI HARA

B.Sc., University of British Columbia, 1959

A THESIS SUBMITTED IN PARTIAL FULFILMENT OF

THE REQUIREMENTS FOR THE DEGREE OF

MASTER OF SCIENCE

in the Department

of

PHYSICS

We accept this thesis as conforming to the

required standard

THE UNIVERSITY OF BRITISH COLUMBIA

October, 1960

In presenting this thesis in partial fulfilment of the requirements for an advanced degree at the University of British Columbia, I agree that the Library shall make it freely available for reference and study. I further agree that permission for extensive copying of this thesis for scholarly purposes may be granted by the Head of my Department or by his representatives. It is understood that copying or publication of this thesis for financial gain shall not be allowed without my written permission.

Department of Physics,

The University of British Columbia,
Vancouver 8, Canada.

Date September 21st, 1960.

ABSTRACT

This thesis describes the design of a magnetometer for recording geomagnetic micropulsations. The nuclear magnetic resonance phenomenon of hydrogen nuclei in water is utilized in the sensing unit of a feedback system, the feedback current being recorded as a measure of the geomagnetic variation. The thesis establishes the feasibility of a feedback system magnetometer.

The system transfer function is derived and from it the sensitivity, stability, steady state error and dynamic range are determined. The dispersion mode signal of nuclear magnetic resonance obtained experimentally is shown and compared with that predicted theoretically. The advantages of a feedback system are indicated. The difficulty in closing the feedback loop is discussed and methods for overcoming this problem are suggested.

TABLE OF CONTENTS

LIST OF ILLUSTRATIONS

ACKNOWLEDGEMENTS

I would like to express my sincere thanks to Professor J.A. Jacobs for encouraging and creating the opportunity to further my knowledge.

Thanks are also due to Dr. J.M. Rocard who suggested the project and helped in many phases of the work, and Dr. D.A. Christoffel for advising in the absence of Dr. Rocard. Much help was gratefully received from the members of the Geophysics Laboratory and Physics Workshop during the construction of the magnetometer.

I also wish to acknowledge the invaluable assistance received from the members of the Nuclear Magnetic Resonance Group through many discussions and demonstrations.

I am indebted to my wife who assisted in all stages of my education and who drew the sketches of the apparatus.

This research project was made possible by a grant from the Geophysics Research Directorate, Air Force Cambridge Research Centre, United States Air Force.

INTRODUCTION

In recent years much attention has been focused on the fine structure of geomagnetic field variations[1][2][3]. Of special interest are micropulsations which have periods in the range 0.1 seconds to 10 minutes. The amplitudes range from a fraction of a gamma (γ)* to, on occasions, as much as several tens of gammas. More theoretical and observational work is required before a satisfactory explanation of the origin of micropulsations can be given, although the source appears to lie in the interaction of solar corpuscular radiation with the geomagnetic field. World wide simultaneous observations with magnetometers of similar characteristics will greatly facilitate the theoretical analysis of micropulsations. A magnetometer with a constant frequency response from DC to above 10 c.p.s. and sensitivity better than one gamma would be extremely useful as a monitor of micropulsations since an accurate comparison of the amplitudes of various fundamental frequencies could be made. If the dynamic range extended up to several hundred gammas, magnetic storms could also be recorded and interesting comparisons with micropulsations would be possible. The magnetometer constructed by the author was designed to fulfill, in part,

---

* 1 γ = 10^{-5} gauss = 10^{-9} weber/m^2.

these desirable characteristics.

Existing methods of measuring micropulsations are the fluxgate (saturable reactor) magnetometer[4], inductive coils[5] and conventional variometers with high amplification. The high frequency response and sensitivity of variometers are limited because of the comparatively large mechanical time constant of the magnet. The fluxgate magnetometer is an excellent device capable of wide frequency response and high sensitivity, although the instability of the core material to mechanical shock, and a steady drift of the base line due to the electronic circuitry, limit the absolute calibration and sensitivity of the magnetometer. Inductive coils have very high sensitivity but their frequency response is not linear and they give the derivative of the geomagnetic field variation.

The well known proton free precession magnetometer[6][7] gives an averaged reading of the geomagnetic field flux density over a period from 0.25 seconds to several seconds, and readings can only be taken at four second or longer intervals. Therefore, it is not suitable for observing micropulsations.

As in several measuring devices[8][9], it is also possible to apply feedback system designs to magnetometers. A feedback system fluxgate magnetometer was successfully constructed by A. Maxwell in 1951[10]. A variometer is also being used for the sensing unit of a feedback system

magnetometer now under consideration in Japan[11]. The application of nuclear magnetic resonance[12] of protons to measure geomagnetic field variations was suggested by J.M. Rocard* in 1958 and the design of a feedback system and construction of the apparatus was undertaken by the author in 1959. A survey of feedback system theory is given in Appendix B and other topics pertinent to the discussion of nuclear magnetic resonance phenomenon are given in Appendix A.

The units widely used to measure geomagnetic flux density are the gauss and gamma (γ) where one gamma is defined as 10^{-5} gauss. The symbol γ is also used to denote the gyromagnetic ratio but in all cases the context will indicate which meaning is intended. Although the m.k.s. system of units is preferred, the system of practical c.g.s. units is used throughout in order to avoid the troublesome conversion of units to obtain the flux density in gauss.

---

* Now at Texas Instruments Inc., Central Research Laboratories, Dallas, Texas, U.S.A.

CHAPTER I

PRINCIPLE OF OPERATION

1.1 Feedback Systems

Closed loop measuring devices utilizing feedback system principles are increasing in number. The reason for this increase is apparent when the advantage of a closed loop system over an open loop system is determined. Consider an idealized open loop measuring system as shown in Fig. (1).

Initially the system is calibrated against a suitable reference. The unknown voltage is then connected to the system and the result suitably displayed.

Since

$$V_2 = K_o V_1 ,$$

it follows that, assuming V_1 constant,

$$\triangle V_2 = V_1 \cdot \triangle K_o .$$

Obviously any variation in gain due to component variation has a direct bearing on the displayed result. Therefore frequent checks on calibration are required for delicate open loop measuring devices.

The performance of a closed loop system is relatively independent of component variations. Consider an idealized measuring device, shown in Fig. (2), utilizing a closed

loop system.

Since

$$\frac{V_1 - V_2}{Z_1} + \frac{V_3 - V_2}{Z_3} = \frac{V_2}{Z_2}$$

and

$$V_3 = K_c V_2 \ ,$$

by eliminating V_2, the following expression is obtained:

$$V_1 = Z_1 V_3 \left\{ \frac{1}{K_c Z_1} + \frac{1}{K_c Z_2} + \frac{1}{Z_3} \left(\frac{1}{K_c} - 1 \right) \right\}$$

For very large K_c,

$$V_3 \approx - \frac{Z_3}{Z_1} \ V_1 \ .$$

Hence amplification is independent of K_c provided K_c is sufficiently large, and any small deviation in K_c will not affect the measuring system. Therefore for a closed loop system to be reliable, only Z_1 and Z_3 need be stable. Identical characteristics of performance can be obtained from several devices based on a closed loop system design by keeping only the components constituting Z_1 and Z_3 to close tolerances.

An example of a potentiometer based on feedback system principles is shown in Fig. (3). The modulator amplitude modulates the carrier frequency according to the magnitude

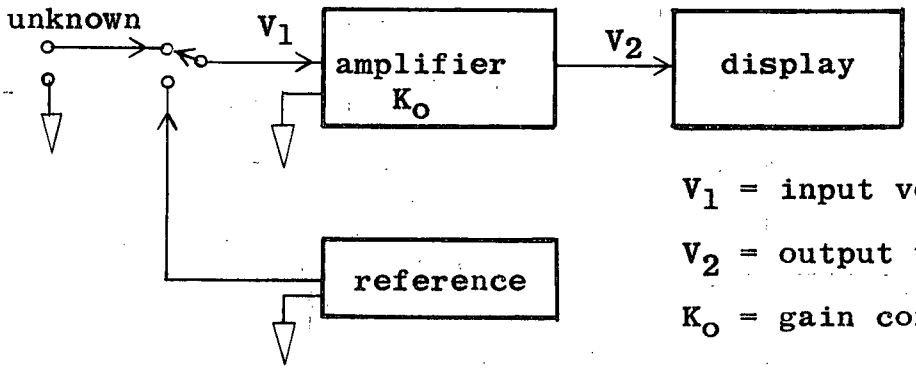

Fig. (1)

Open Loop Measuring System.

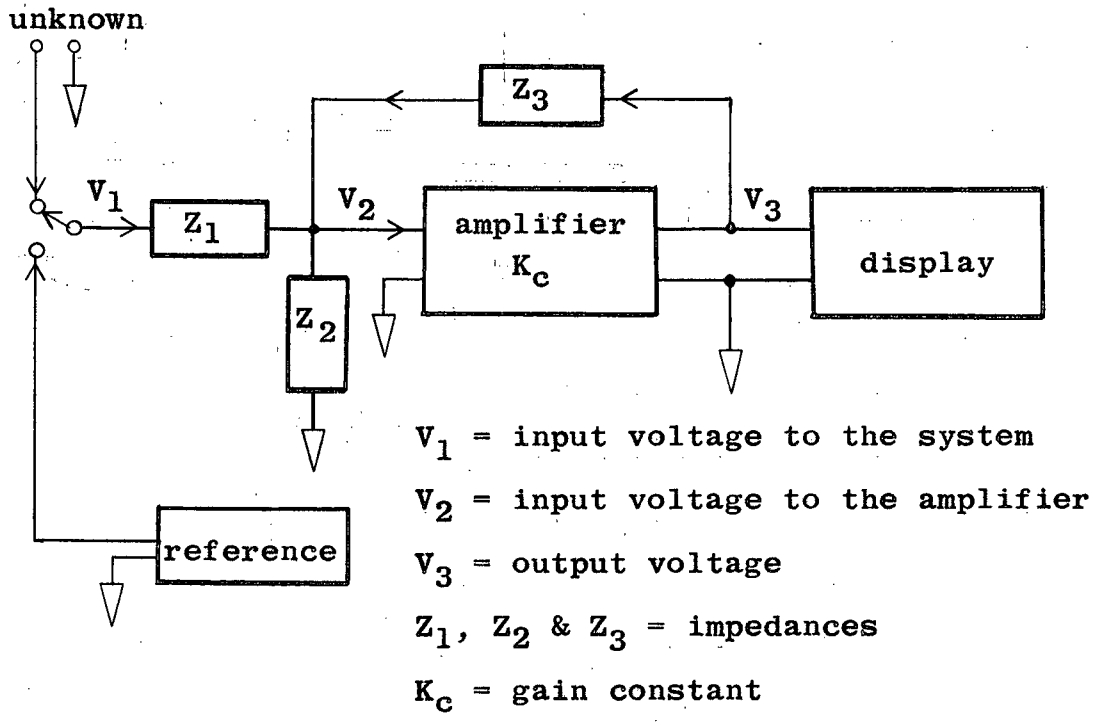

Fig. (2)

Closed Loop Measuring System.

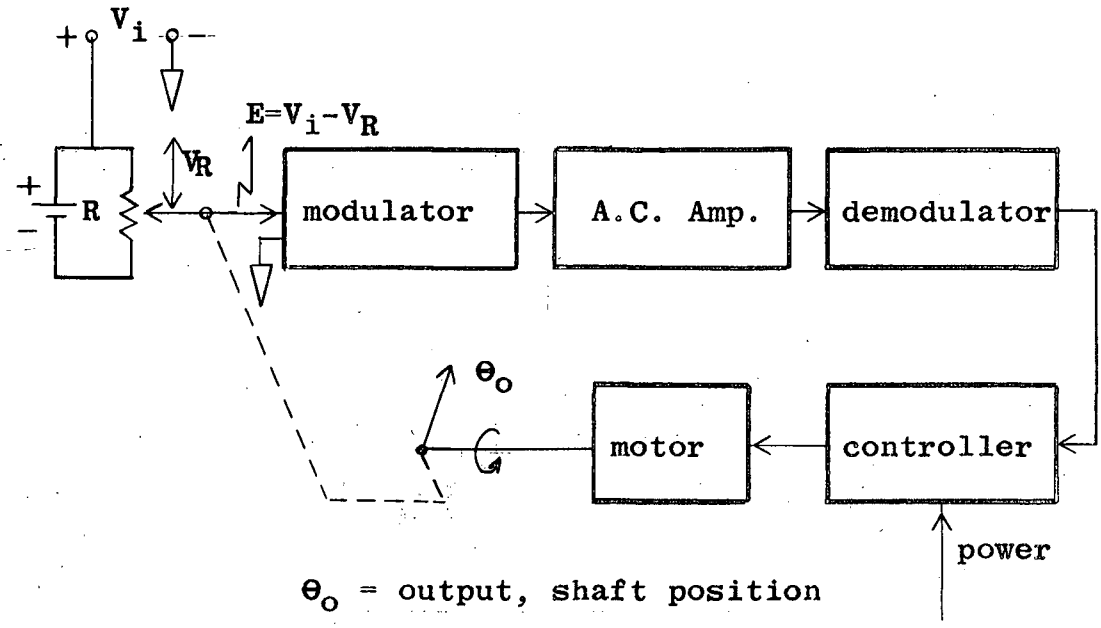

θ_o = output, shaft position

V_i = input voltage to system

V_r = potentiometer voltage

E = error voltage

Fig. (3)

Feedback System Potentiometer.

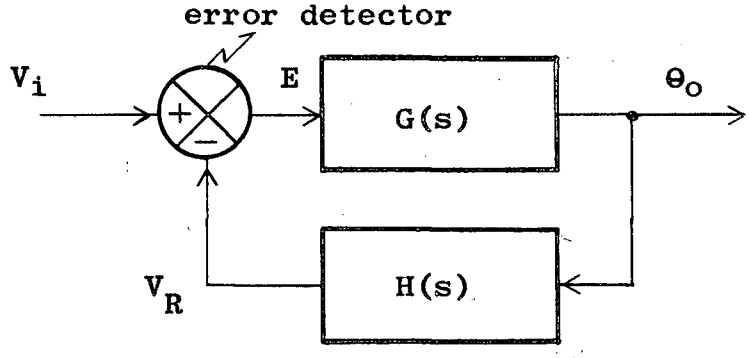

G(s) = forward transfer function

H(s) = feedback transfer function

Fig. (4)

Equivalent Block Diagram of the Potentiometer.

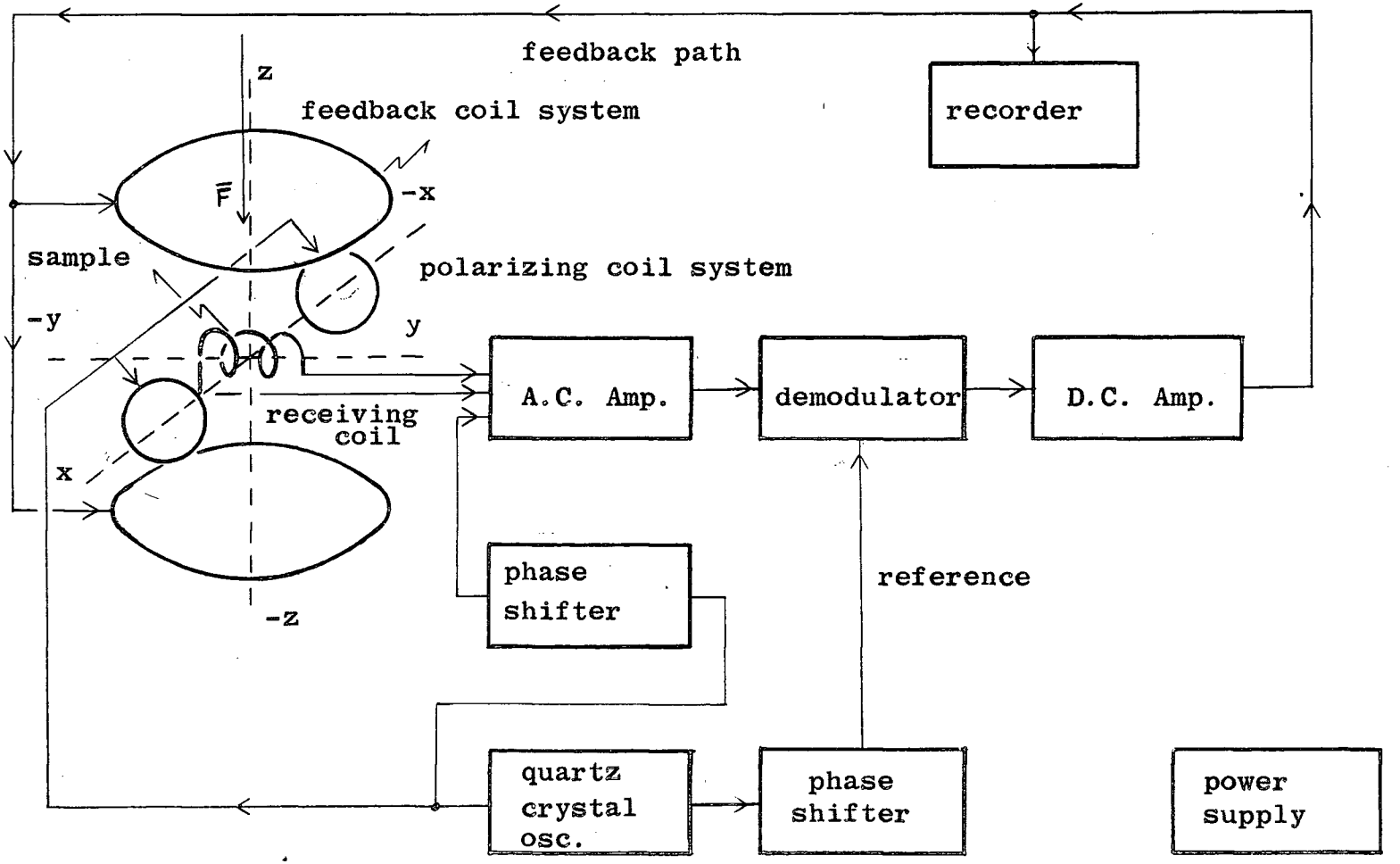

Fig. (5)

The Nuclear Magnetic Resonance Proton Magnetometer.

and polarity of the error voltage E. E is the difference in voltage between input voltage V_1 and potentiometer voltage V_R. After amplification and demodulation, the motor is caused to rotate according to the magnitude and polarity of E. The motor shaft rotates the moving arm of the variable resistor R in such a way as to reduce E to zero. The final shaft position gives the magnitude of the voltage V_1.

In terms of feedback system analysis the block diagram of the system shown in Fig. (3) is given in Fig. (4). The transfer function of the system is given by*

$$Y(s) = \frac{G(s)}{1+G(s)H(s)}$$

where s corresponds to the complex angular frequency jw and the equation given is in the Laplace transform space. The output is given by

$$\theta_o(t) = L^{-1}\left\{V_i(s)Y(s)\right\}$$

1.2 Block Diagram

A block diagram of the proton resonance magnetometer is shown in Fig. (5). Briefly, it is a carrier feedback system where the magnitude of the geomagnetic field $\overline{F}$ is maintained essentially at a constant value throughout the

---

* See Appendix B, Sec. 4.

water sample by the feedback system. The carrier is supplied by the precessing protons, and modulation of the carrier accomplished by the variation of the geomagnetic field through the mechanism of nuclear magnetic resonance*.

The modulated carrier is amplified through a narrow band A.C. amplifier and the demodulator (phase sensitive detector) detects the magnitude and polarity of the geomagnetic field variation. The detected output is then amplified by a D.C. amplifier, the output current of which is passed through a Helmholtz coil system to cancel the variation of the geomagnetic field, thereby closing the negative feedback loop. The magnitude of the feedback current is recorded as an indication of the geomagnetic field variation. The quartz crystal oscillator supplies the reference to the demodulator and also provides a linearly oscillating field $\overline{H}_p$ through the polarising Helmholtz coil system to produce the nuclear magnetic resonance phenomenon of the hydrogen protons in the water sample.

1.3 Signal

A model of Bloch, Hansen and Packards'[13] crossed coil nuclear induction apparatus is shown in Fig. (6). The proton resonance magnetometer has a similar configuration, as in Fig. (5).

---

* See Appendix A, Sec. 2.

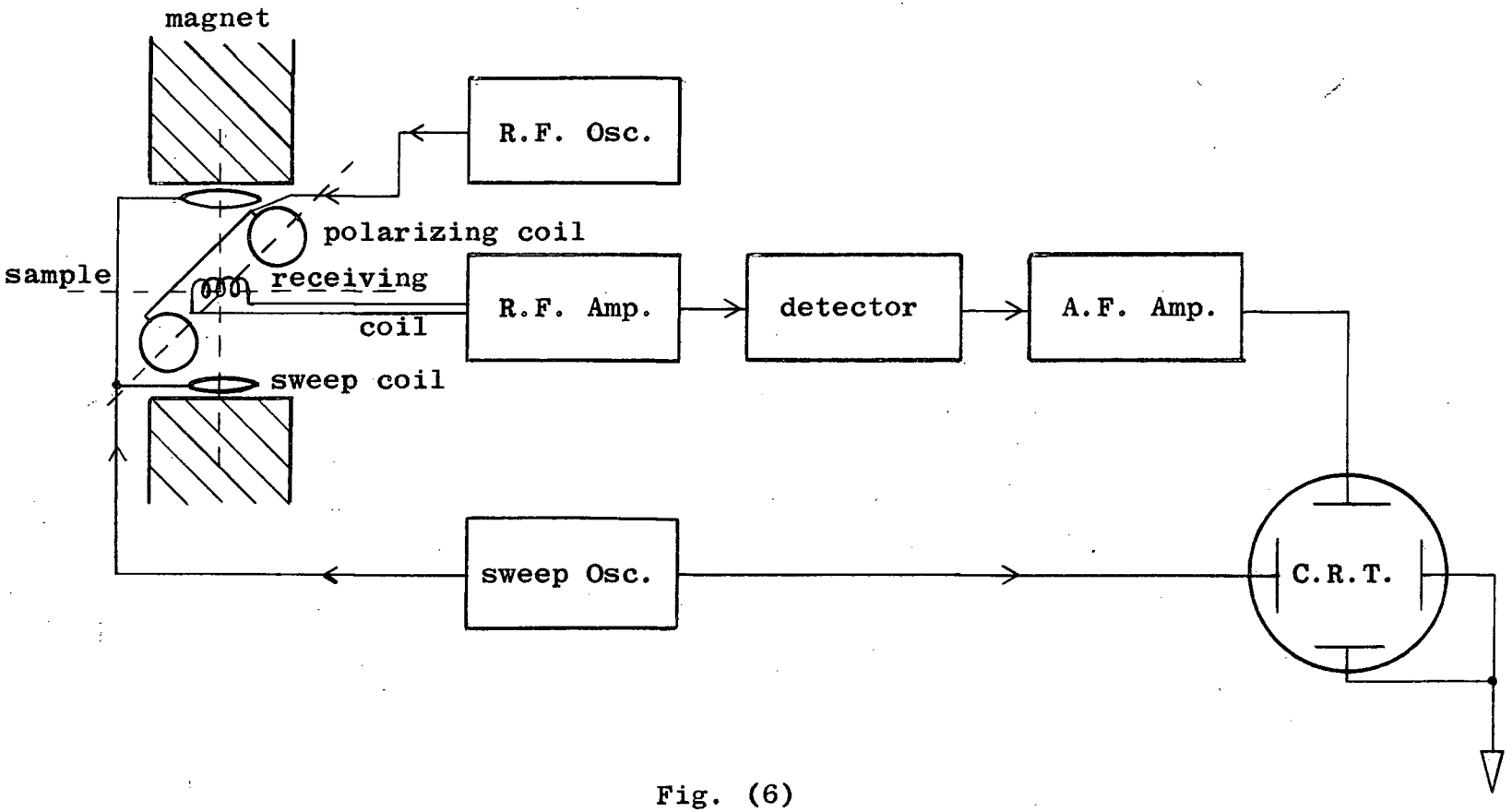

Fig. (6)

Crossed Coil Nuclear Induction Experiment.

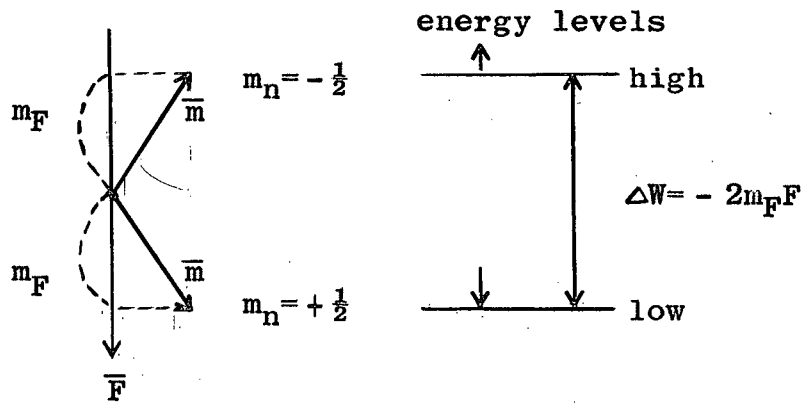

Fig. (7)

Energy States of Protons.

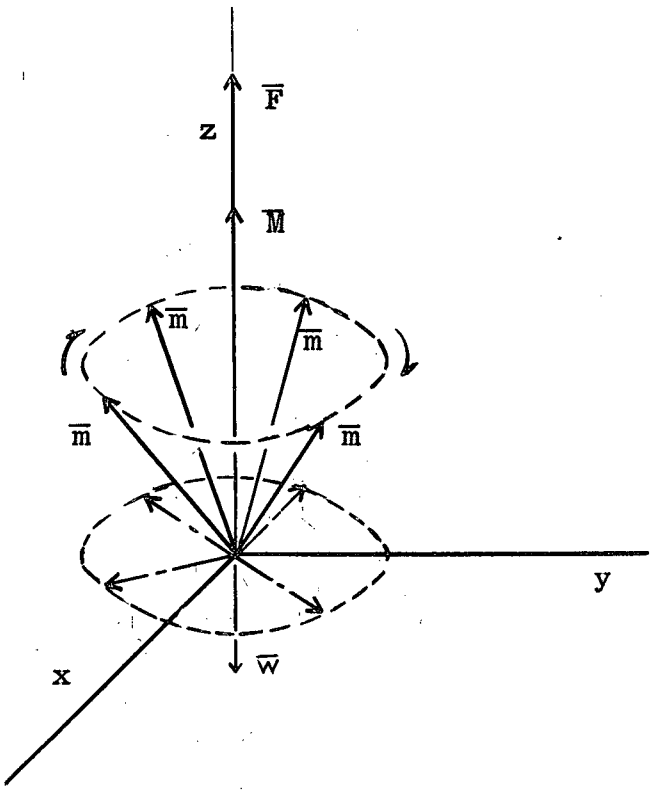

Fig. (8)

No x and y Components of $\overline{M}$.

The sample in the case of the magnetometer is water, a diamagnetic substance. The oxygen 16 nucleus has zero effective magnetic moment and the nucleus of hydrogen, the proton, has a magnetic moment $\overline{m}$. Throughout this thesis, for convenience, the hydrogen nucleus will be simply referred to as the proton. The electrons contribute no net magnetic moment. Because of the relatively large internuclear distance and electron to nucleus distance, it is reasonable to assume that the protons are essentially non-interacting free particles, and in the absence of any external magnetic field, the magnetic moments are oriented randomly so that no net magnetic moment exists for the sample.

When an external magnetic field $\overline{F}$ is applied, the proton magnetic moments $\overline{m}$ tend to align along the $\overline{F}$ direction. Due to quantization, protons have magnetic quantum numbers $m_n = \pm \frac{1}{2}$, and only two quantum states are allowed as indicated in Fig. (7). The physically observable component of $\overline{m}$, is given by

$$m_F = \frac{\overline{m} \cdot \overline{F}}{F} \quad .$$

For a proton, where the gyromagnetic ratio is positive, the favourable (lower) energy state is $m_n = +\frac{1}{2}$. The requirement of thermal equilibrium between the spin system and "lattice" prevents part of the proton magnetic moments from assuming the $m_n = +\frac{1}{2}$ state, and the equilibrium condition established is the Boltzmann Distribution:

$$\frac{N(m_n = +\frac{1}{2})}{N(m_n = -\frac{1}{2})} = \exp\left(-\frac{\Delta W}{kT}\right) \approx 1 + \frac{2m_F F}{kT}$$

where ΔW = $-2m_F F$, the energy difference of the two states

$N(m_n)$ = the number of protons in energy state m_n

k = Boltzmann's Constant

T = absolute temperature of the "lattice"

and $\frac{2m_F F}{kT} \cdot N(m_n = -\frac{1}{2})$ = the excess number of protons in $m_n = +\frac{1}{2}$ energy state.

Obviously any change in the external magnetic field or temperature will be met by dissipation or absorption of energy by the proton assembly as a whole and a new equilibrium state will be eventually established. The mechanism of transfer of energy to and from the protons is known as the longitudinal, thermal or spin-lattice relaxation effect and a time constant T_1 is associated with this effect. T_1 is a measure of the time required for the protons to establish thermal equilibrium with the "lattice".

Since the proton has an intrinsic spin, the external magnetic field $\overline{F}$ acting on the magnetic moment $\overline{m}$ of the proton causes $\overline{m}$ to precess about $\overline{F}$. The angular velocity $\overline{w}$ of precession is given by

$$\overline{w} = -\gamma \overline{F}$$

where $\overline{m} = \gamma \overline{a}$

γ = the gyromagnetic ratio*

and $\overline{a}$ = the angular momentum of a proton.

---

* For protons $\gamma = (2.67528 \pm 0.00006) \times 10^4$ sec^{-1} gauss^{-1}. Throughout this thesis γ will be considered as positive.

The Larmor precession frequency f is then

$$f = \frac{1}{2\pi} \gamma F \ .$$

At thermal equilibrium the magnetic moments precess about $\overline{F}$ with incoherent phase at frequency f. Since there is a slight excess of protons in the $m_n = +\frac{1}{2}$ state, a macroscopic resultant magnetization vector $\overline{M}$ exists along the direction of $\overline{F}$. Because of the incoherent phase of precession of the excess proton magnetic moments, all components in directions perpendicular to $\overline{F}$ cancel, as in Fig. (8), and no signal is induced in the receiver coil aligned along the y axis.

Consider the crossed coil system shown in Fig. (5). An oscillating magnetic field $\overline{H}_p = 2\overline{H}_1 \cos w_r t$ is applied along the x axis, perpendicular to the external magnetic field $\overline{F}$ which is parallel to the z axis. For convenience let $\overline{H}_p$ be expressed by two counter rotating magnetic fields given by

$$\begin{cases} H_x = H_1 \cos w_r t \\ H_y = H_1 \sin w_r t \end{cases} \qquad (1\text{-}1)$$

and

$$\begin{cases} H_x = H_1 \cos w_r t \\ H_y = -H_1 \sin w_r t \end{cases} \qquad (1\text{-}2)$$

Referring to Fig. (8), if $\overline{F}$ approaches the resonance value $\overline{H}_r$ where

$$-\gamma \overline{H}_r = \overline{w}_r$$

the rotating component (1-2) of $\overline{H}_p$ will become synchronus with the precessing proton magnetic moments $\overline{m}$ of the sample. Then, it can be readily shown that the difference in the number of protons in the two $m_n = \pm\frac{1}{2}$ energy states is decreased because of the "flipping" of the magnetic moments into the higher $m_n = -\frac{1}{2}$ energy state*. Energy is absorbed by the proton from the polarizing field $\overline{H}_p$ in the process. Thus the resultant macroscopic magnetization $\overline{M}$ in the z axis direction is reduced.

In addition, the precessing proton magnetic moments experience a torque $\overline{T}$ expressed by

$$\overline{T} = \frac{d\overline{a}}{dt} = \overline{m} \times \overline{H}_1$$

where $\overline{H}_1$ is the rotating component of $\overline{H}_p$. Consequently, as shown in Fig. (9), the macroscopic resultant magnetization vector $\overline{M}$ is tipped away from, and precesses about, the z axis. In effect, $\overline{H}_1$ tends to tip the magnetic moments as well as group them together so that they precess with coherent phase, and the result produces the precessing macroscopic magnetization vector. Thus there are now components M_x and M_y of the macroscopic magnetization vector in the xy plane. The M_y component induces, in the receiving coil, an e.m.f. which is the nuclear magnetic resonance signal of protons in the sample.

---

* See Appendix A, Sec. 2

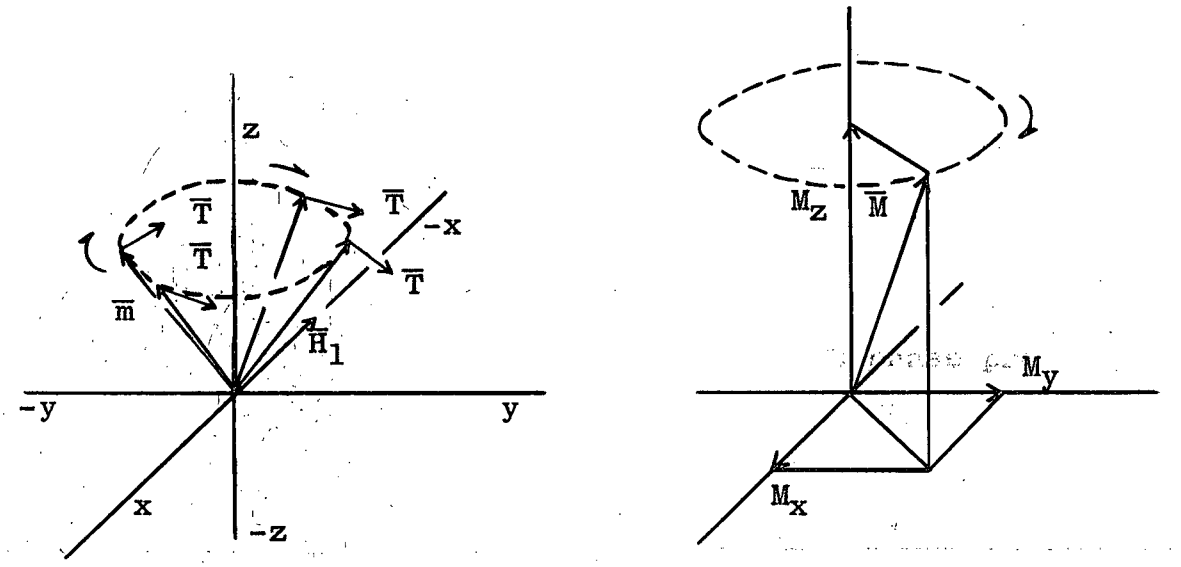

incoherent phase precession

coherent phase precession

Fig. (9)

Magnetic Resonance Producing M_x and M_y.

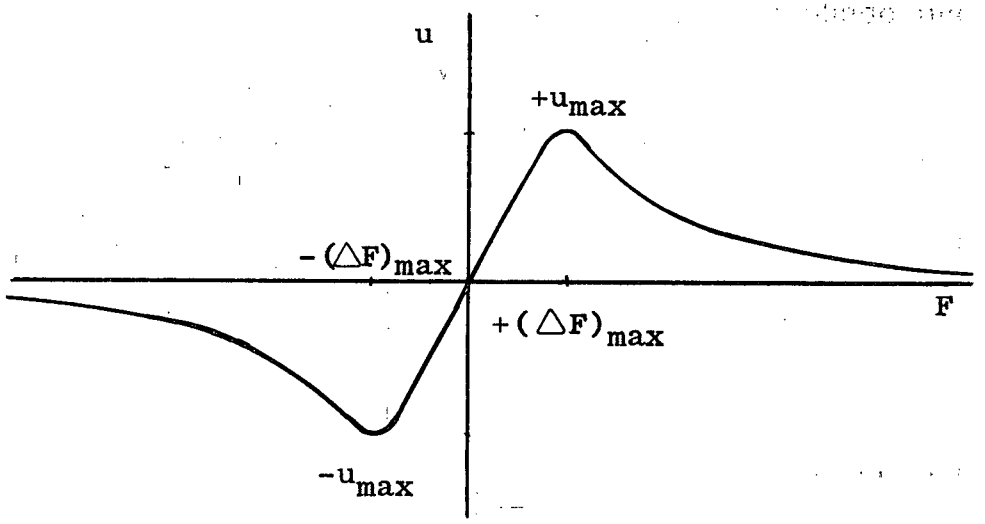

Fig. (10)

u-mode Signal Amplitude.

The effect of the rotating component (1-1) of $\overline{H}_p$ is negligible in most cases[14].

The magnitude of M_y depends on two equilibrium conditions of the resultant magnetization vector $\overline{M}$. The first is the spin-lattice relaxation effect, discussed previously, with associated time constant T_1. The second is the transverse, or spin-spin relaxation effect with associated time constant T_2^*. Spin-spin relaxation takes place through the interaction of the precessing proton magnetic moments, by the exchange of energy among themselves. The inhomogeneity of $\overline{F}$ over the sample also contributes to the spin-spin relaxation by producing minor differences in the precession frequency of the protons in the sample. In other words T_2^* is a measure of the time taken for a group of precessing magnetic moments initially in phase with each other to become out of phase.

It is readily shown that for a constant external magnetic field $\overline{F}$, the macroscopic magnetization vector M_y is given by*

$$M_y = -(u \sin w_r t + v \cos w_r t) \qquad (1\text{-}3)$$

where

$$u = \frac{H_1 M(\gamma T_2^*)^2}{1 + (\gamma H_1)^2 T_1 T_2^* + (\gamma T_2^*)^2 (F - H_r)^2} \qquad (1\text{-}4)$$

---

* See Appendix A, Sec. 3

$$v = \frac{H_1 M \gamma T_2^*}{1 + (\gamma H_1)^2 T_1 T_2^* + (\gamma T_2^*)^2 (F-H_r)^2} \qquad (1\text{-}5)$$

γ = gyromagnetic ratio

M = magnetic moment per unit volume, $M = XH_r$

X = paramagnetic susceptability of protons

H_r = magnitude of external field where magnetic resonance takes place

H_1 = $\frac{1}{2}$ maximum value of the polarizing field $\overline{H}_p$

F = external magnetic field

T_1 = spin lattice relaxation time

and T_2^* = transverse relaxation time .

Bloch[15] has pointed out that for time dependent variation of $\overline{F}$, equation (1-3) still holds provided

$$\left| \frac{d}{dt}\left(\frac{w-w_r}{H_1}\right) \right| \ll \gamma H_1 ,$$

where $w = \gamma F$

and $w_r = \gamma H_r$.

In other words,

$$\left|\frac{dF}{dt}\right| \ll \gamma H_1^2 \qquad (1\text{-}6)$$

must be satisfied. In Chapter III it is shown that this condition is satisfied.

The magnetic flux Φ through a solenoidal coil of cross

section area A, with N turns is

$$\Phi = 4\pi\ NAM_y = -4\pi\ NA\ (u \sin w_r t + v \cos w_r t)\ .$$

Assuming that $\Delta F = F - H_r$ is almost constant so that its time derivative is negligible , the induced e.m.f. V_1 across the terminals of the coil is given by

$$V_1 = -\frac{1}{c}\frac{d\Phi}{dt} = \frac{1}{c}\ 4\pi\ NAw_r\ (u \cos w_r t - v \sin w_r t)$$

where c = velocity of light.

However, in practice the coupling between the polarizing coil system and receiver coil is not zero and some leakage of $\overline{H}_p$ occurs. The leakage component along the y axis is expressed as

$$H_y = h \cos w_r t\ ,$$

where h is a constant factor dependent on the geometry of the coil system. Therefore, the signal induced in the receiver coil is actually,

$$V_1 = \frac{1}{c}\ 4\pi\ NA\ w_r \left\{u \cos w_r t - (v-h) \sin w_r t\right\} \qquad (1\text{-}8)$$

The effect of the leakage H_y will be considered in Chapter IV.

1.4 Error Detector Modulator

In 1.1 the magnetometer was referred to as a carrier

feedback system. The modulated carrier is the signal appearing across the receiver coil, expressed by equation (1-8). Since the demodulator is insensitive to quadrature components* either of the two sinusoidal terms in equation (1-8) may be selected**. To detect the magnitude and direction of the variation of the external magnetic field $\overline{F}$, the u cos wt term must be chosen. Consider the signal

$$S_u = u \cos wt = \frac{H_1 M (\gamma T_2^*)^2 \{F(t)-H_r\} \cos w_r t}{1 + (\gamma H_1)^2 T_1 T_2^* + (\gamma T_2^*)^2 \{F(t)-H_r\}^2} \qquad (1\text{-}9)$$

which is referred to as the u-mode signal. Inspection of equation (1-8) and (1-9) shows that the carrier frequency f_c is

$$f_c = \frac{w_r}{2\pi}$$

and that the amplitude u of the carrier cos $w_r t$ is a function of

$$\triangle F = F(t)-H_r \quad .$$

At resonance, $F = H_r$ and $S_u = 0$.

The general form of the amplitude u as a function of $\triangle F$ is shown in Fig. (10). It is readily shown that***,

---

* See 1.6

** Note that we have a linear system and, therefore, the Superposition Principle holds and any signal may be treated term by term.

*** See Appendix A, Sec. 3

$$u = u_{mx} = \frac{\gamma H_1 T_2^* M}{2\left\{1 + (\gamma H_1)^2 T_1 T_2^*\right\}^{\frac{1}{2}}} \qquad (1\text{-}10)$$

when

$$\triangle F = \pm \frac{1}{\gamma T_2^*} \left\{1 + (\gamma H_1)^2 T_1 T_2^*\right\}^{\frac{1}{2}} \qquad (1\text{-}11)$$

It is apparent that the direction of the deviation of F from the resonance value H_r is expressed by the u-mode signal, and although non-linear, the magnitude of the deviation of F is also contained as the amplitude in the u-mode signal. Therefore, the u-mode signal of the proton resonance provides the error detector and amplitude modulator required of a carrier feedback system. The non-linearity of the amplitude modulation is not serious since the negative feedback allows only a small portion of the curve in the neighbourhood of $\triangle F = 0$ to be used which can be considered linear. The manner in which amplitude modulation takes place is shown graphically in Fig. (11). The error detector and modulator have an associated transfer function approximately equal to a constant gain factor K_1. The approximation will be discussed in Chapter III.

The block diagram in Fig. (5) can now be redrawn as shown in Fig. (12).

1.5 A.C. Amplifier

The A.C. amplifier (carrier amplifier) is a narrow band

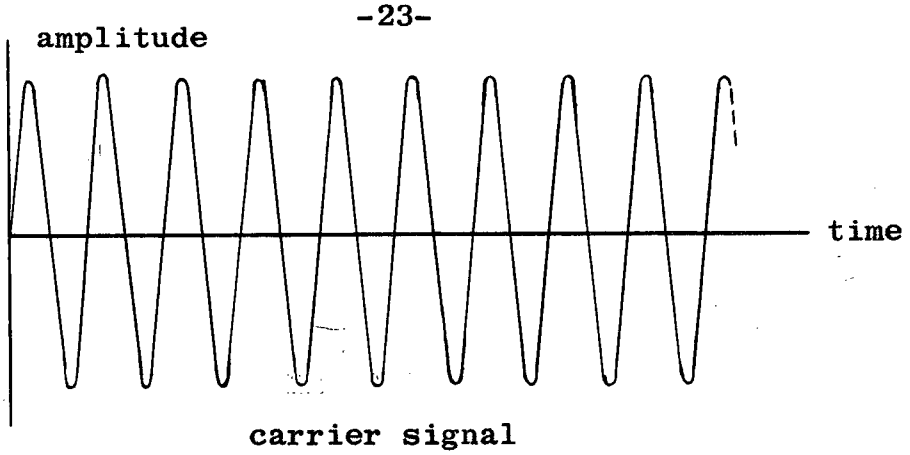

carrier signal

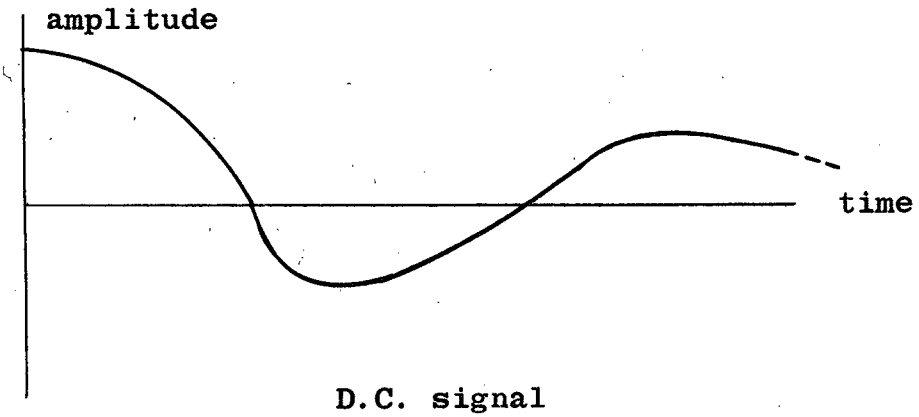

D.C. signal

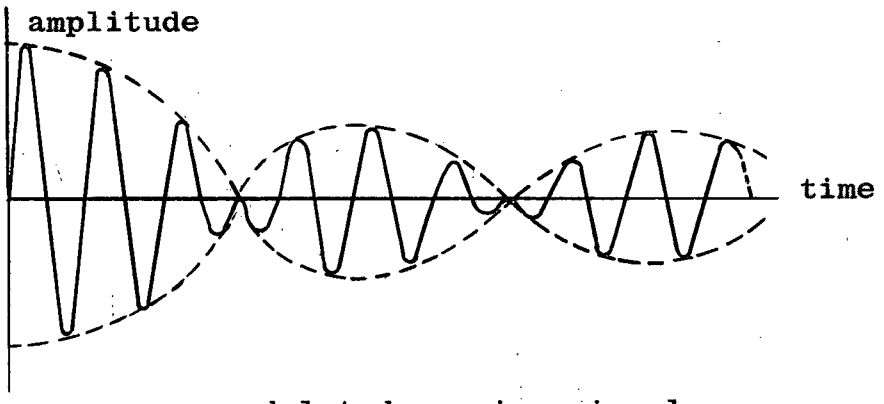

modulated carrier signal

Note the abrupt 180° phase change where F = H_r.

Fig. (11)

Operation of the Modulator.

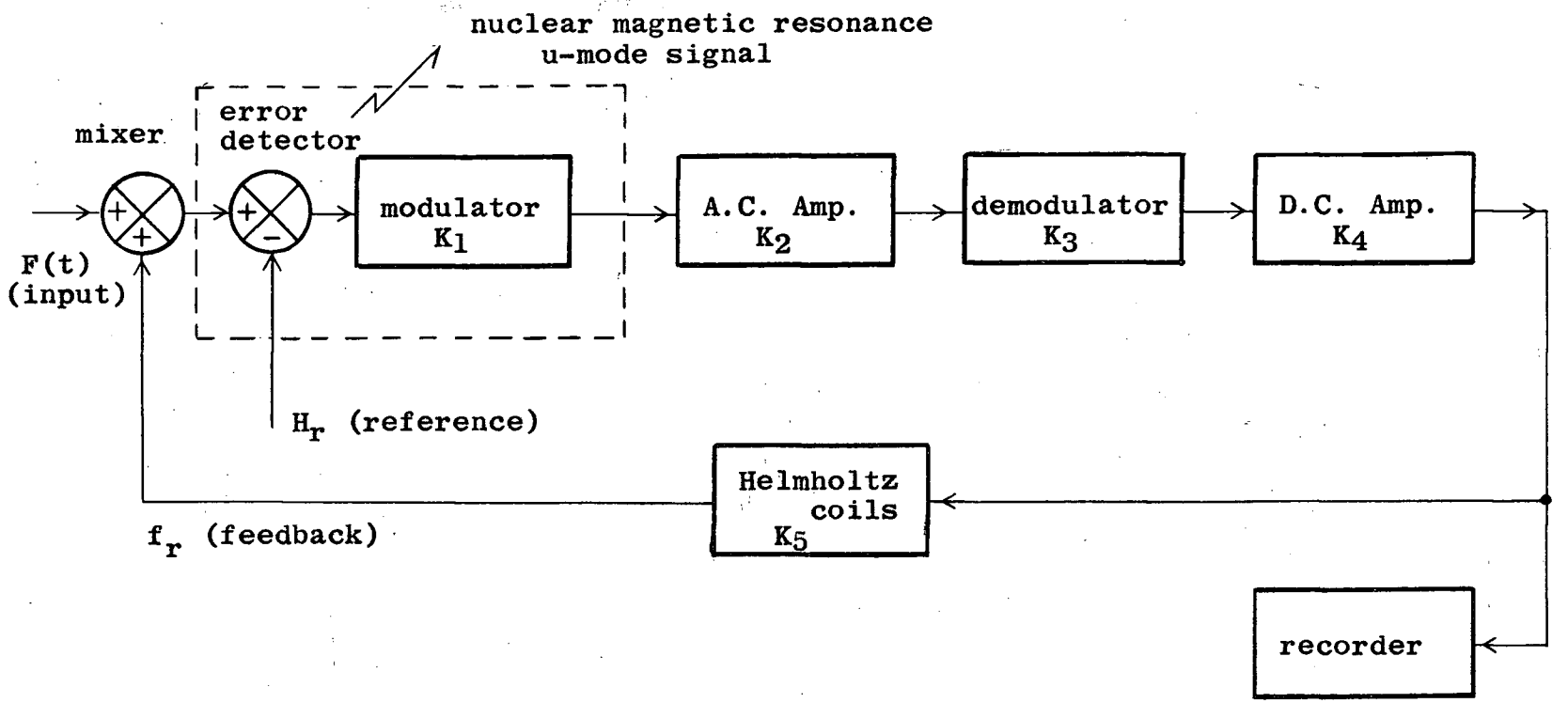

Fig. (12)

Block Diagram of the Nuclear Magnetic Resonance Proton Magnetometer.

amplifier with center frequency f_c approximately equal to the Larmor precession frequency of the protons subjected to the main geomagnetic field. The form of the frequency response of the amplifier is shown in Fig. (13). In order to prevent the "ringing" of the high quality factor resonance filters by 60 c.p.s. noise, 60 c.p.s. rejection "Twin T" circuits are inserted. The rejection circuits cause the dip at 60 c.p.s. in Fig. (13).

For simplicity consider the case where the carrier signal $\cos w_r t$ is modulated by A cos Wt. The modulated carrier signal is,

$$A \cos Wt \cos w_r t = \frac{A}{2} \cos (W+w_r)t + \cos (W-w_r)t \ .$$

Since the carrier frequency $f_c = \frac{w_r}{2\pi}$ is absent in the modulated carrier signal, it is referred to as a "suppressed carrier signal". The frequencies of geomagnetic variations that are to be detected extend from 0 to 20 c.p.s. Therefore, sidebands of the modulated carrier over the range $f_s = f_c \pm 20$ c.p.s. must be amplified satisfactorily. For $f_c = 2000$ c.p.s., f_s will be 2020 c.p.s. and 1980 c.p.s., only one percent to each side of f_c. Therefore, no difficulty is encountered when simple parallel resonance circuits are employed.

The transfer function of the A.C. amplifier becomes a constant gain factor K_2 since the amplifier itself has zero

gain at low frequencies, and the frequency response within one percent of the center frequency f_c is essentially constant. Frequencies higher than 20 c.p.s. will be attenuated by the filter associated with the demodulator, if not attenuated by the A.C. amplifier. At most, the A.C. amplifier contributes a phase shift to the signal of geomagnetic variation.

1.6 Demodulator

The function of a demodulator (phase sensitive detector) is to operate upon an amplitude modulated carrier signal to provide a voltage that is proportional to the amplitude of modulation and the polarity of the modulation applied to the carrier signal. The phase of the modulated carrier signal is compared with that of an unmodulated reference signal at carrier frequency. The output is a D.C. voltage which is of one polarity when the modulated carrier and reference are in phase, and of opposite polarity when they are 180° out of phase. If the two are 90° out of phase the output is zero, as shown below.

All demodulators and modulators can be considered as switching devices with suitable filters. Consider the idealized full wave demodulator in Fig. (14). The ideal switching operation can be expressed by a train of square waves shown in Fig. (15) and expressed in terms of a Fourier series as

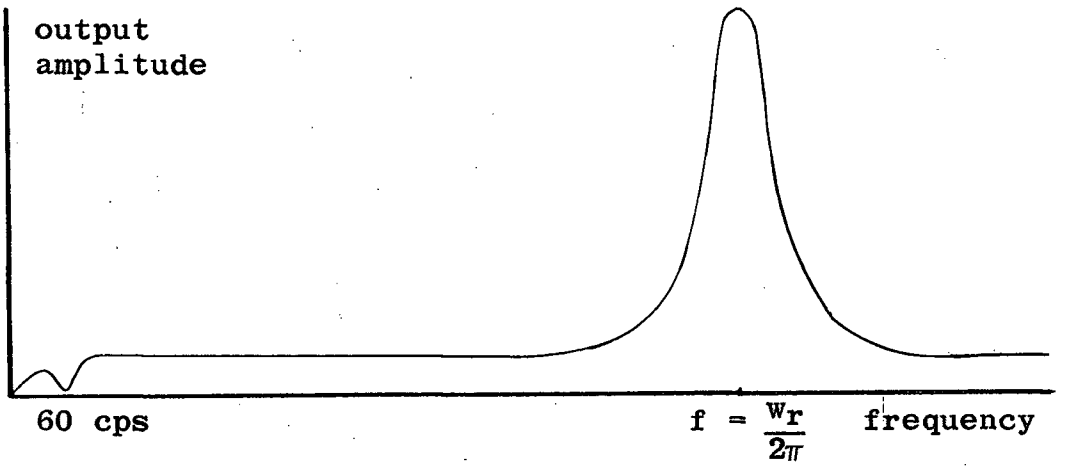

Fig. (13)

A.C. Amplifier Frequency Response.

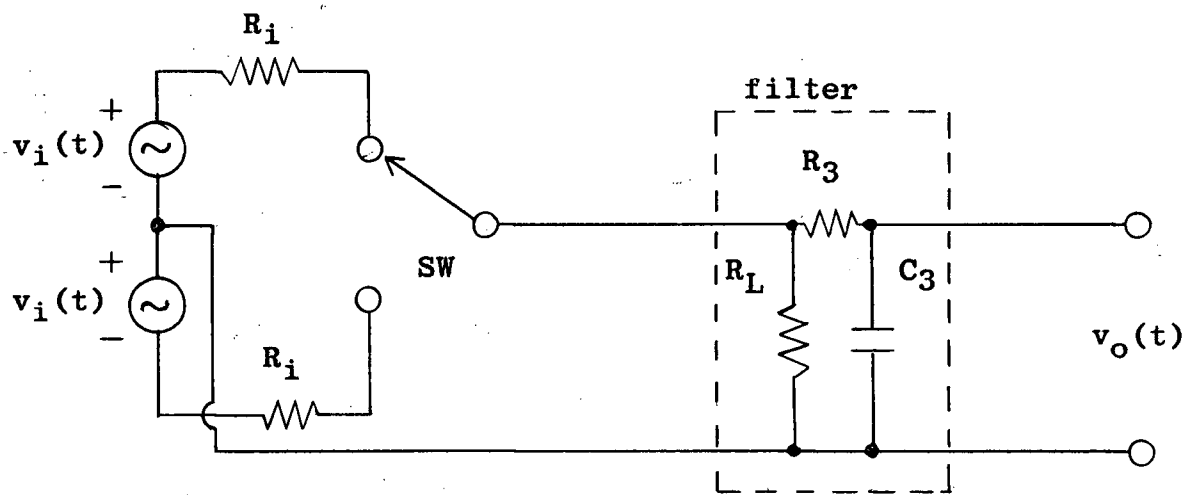

$v_i(t)$ = input voltage

$v_o(t)$ = output voltage

R_i = internal resistance of input voltage source

R_L = load resistor

R_3C_3 = filter; $R_3C_3 = T_3$, time constant of filter

SW = ideal switching device

Fig. (14)

Ideal Demodulator.

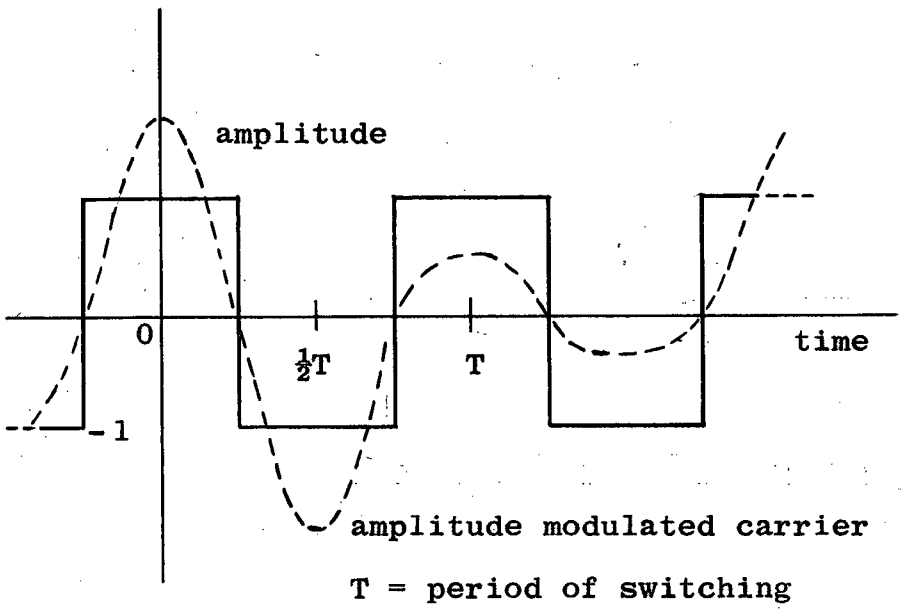

Fig. (15)

Ideal Switching Action.

$$g(t) = \frac{4}{\pi}\left(\cos w_r t - \frac{1}{3}\cos 3 w_r t + \frac{1}{5}\cos 5 w_r t - + \ldots\right)$$

where $w_r = \frac{1}{T}$, and T is the period of the reference frequency.

The input v_i is a carrier modulated signal expressed by

$$v_i(t) = f(t) \cos (w_r t + \theta)$$

where f(t) is the amplitude modulation and cos $(w_r t + \theta)$ is the carrier signal. $v_i(t)$ is essentially in phase with the switching operation. θ accounts for the phase difference between the reference and carrier signal. In practice θ is varied through a phase shift network so that the u-mode signal is chosen accurately. The output from the switch is then, neglecting the attenuation by internal resistance R_i,

$$\begin{aligned} f(t)\cos(w_r t+\theta)g(t) = \frac{4f(t)}{\pi}\Big\{ & \cos w_r t \cos(w_r t+\theta) \\ & -1/3 \cos 3w_r t \cos(w_r t+\theta) \\ & +1/5 \cos 5w_r t \cos(wt+\theta) \\ & - + \ldots \Big\} \end{aligned}$$

$$\begin{aligned} = \frac{2f(t)}{\pi}\Big\{ & \cos\theta + \cos(2w_r t+\theta) \\ & -1/3 \cos(4w_r t+\theta) + \cos(2w_r t-\theta) \\ & +1/5 \cos(6w_r t+\theta) + \cos(4w_r t-\theta) \\ & - + \ldots \Big\} \end{aligned}$$

After passing through a low pass filter the output becomes

$$v_o(t) \approx \frac{2}{\pi} K_3 \cos\theta\, f(t) .$$

K_3 is the gain constant associated with the demodulator as a whole. It is apparent now that, if the phase difference θ between the carrier and reference is $\pm$ 90°, the output is zero. In other words the demodulator is insensitive to quadrature components in the carrier signal. For detection of the u-mode signal, θ is set to zero and the result is

$$v_o(t) \approx K_3 f(t) \quad .$$

The operation of the demodulator is shown graphically in Fig. (16).

The demodulator configuration given is usually referred to as a phase sensitive detector in the sense that it detects the abrupt 180° phase change of the carrier and gives the polarity of the modulation signal f(t). The filter is designed to eliminate all high frequencies. The time constant T_3 is relatively large and will have effects on the low frequencies. Therefore, the transfer function of the demodulator is given as

$$Y_3(s) = \frac{K_3}{sT_3 + 1} \quad ,$$

where $T_3 = R_3C_3$ is the time constant of the demodulator. The derivation is discussed in Chapter III.

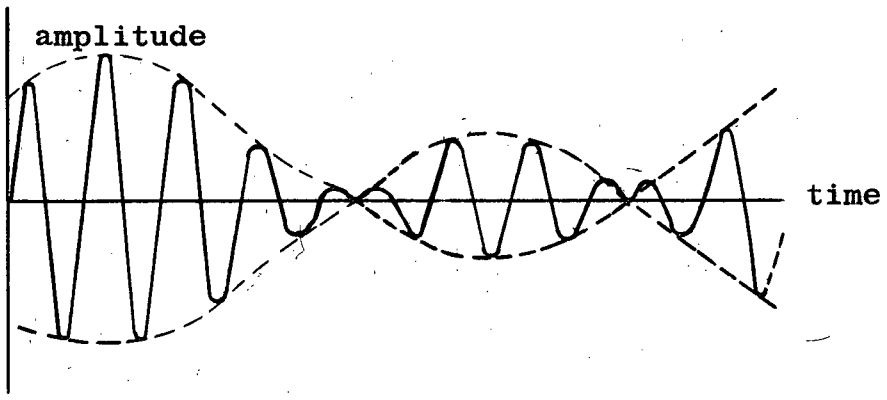

modulated carrier signal

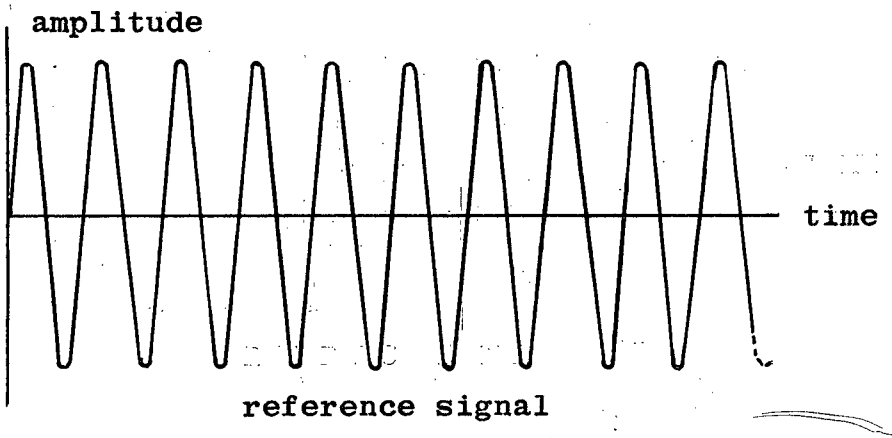

reference signal

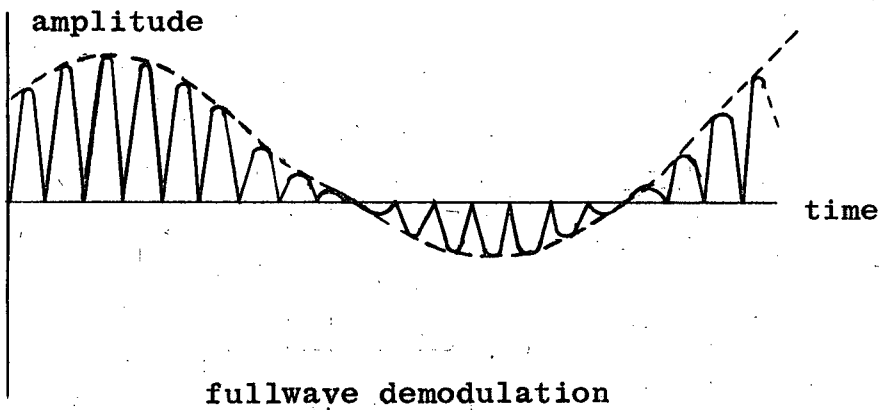

fullwave demodulation

Fig. (16)

Operation of the Demodulator.

1.7 D.C. Amplifier and Feedback Coil System

The D.C. amplifier has a constant frequency response from 0 to several thousand c.p.s. Therefore, the transfer function is a gain constant K_4. The output of the D.C. amplifier is in terms of current and this is recorded as an indication of the geomagnetic variation ΔF.

A Helmholtz coil system closes the negative feedback loop by generating a magnetic field to cancel out ΔF throughout the sample. The inductance of the coil is negligible, since the frequency of interest is very low. Thus the transfer function of the feedback coil system is a constant K_5.

1.8 Summary

The magnetometer is a carrier feedback system with a forward transfer function of the form

$$KG(s) = K_1K_2K_3K_4G_3(s) ,$$

where $G_3(s) = \frac{1}{sT_3+1}$, and a feedback transfer function K_5.

The error detector and modulator have a special form due to the nature of the nuclear magnetic resonance effect. The error signal $v_1(t)$ is given by the error detector and modulator as,

$$v_1(t) = \frac{1}{c}\, 4\pi NA w_r \frac{H_1 M(\gamma T_2^*)^2 \left\{ F(t)-H_r \right\}}{1+(\gamma H_1)^2 T_1 T_2^* + (\gamma T_2^*)^2 \left\{ F(t)-H_r \right\}^2} \cos w_r t$$

The closed loop transfer function is

$$Y(s) = \frac{KG(s)}{1 + K_5 KG(s)} \quad ,$$

and the current recorded is given by

$$i(t) = L^{-1} \left\{ F(s)\ Y(s) \right\} \quad ,$$

where F(s) is the Laplace transform of F(t).

CHAPTER II

DESCRIPTION OF APPARATUS

The basic circuit diagram of the magnetometer is shown in Fig. (17). Sketches of the crossed coil system, rack mounted units and power supply are given in Figs. (18), (19), and (20) respectively. Detailed description of the apparatus is given in the technical manual, which has been written in conjunction with this thesis, and only points of interest are discussed here.

2.1 Power Supply

In order to minimize noise, the power supply is constructed as a separate unit and placed at a distance from the rack mounted units. Most of the vacuum tubes are connected in series and energized by a 300 mA 320 V stabilized source. Vacuum tubes not included in the series heater arrangement and the crystal oven are energized by low voltage D.C. sources. Therefore, in the electronics system proper no 60 cps mains power appears, thus eliminating the time consuming effort of "hum tracing" which is usually required in high gain circuits. There are three independent high voltage regulated power supplies and a regulated bias power supply. By using separate high voltage supplies to the quartz crystal oscillator, phase

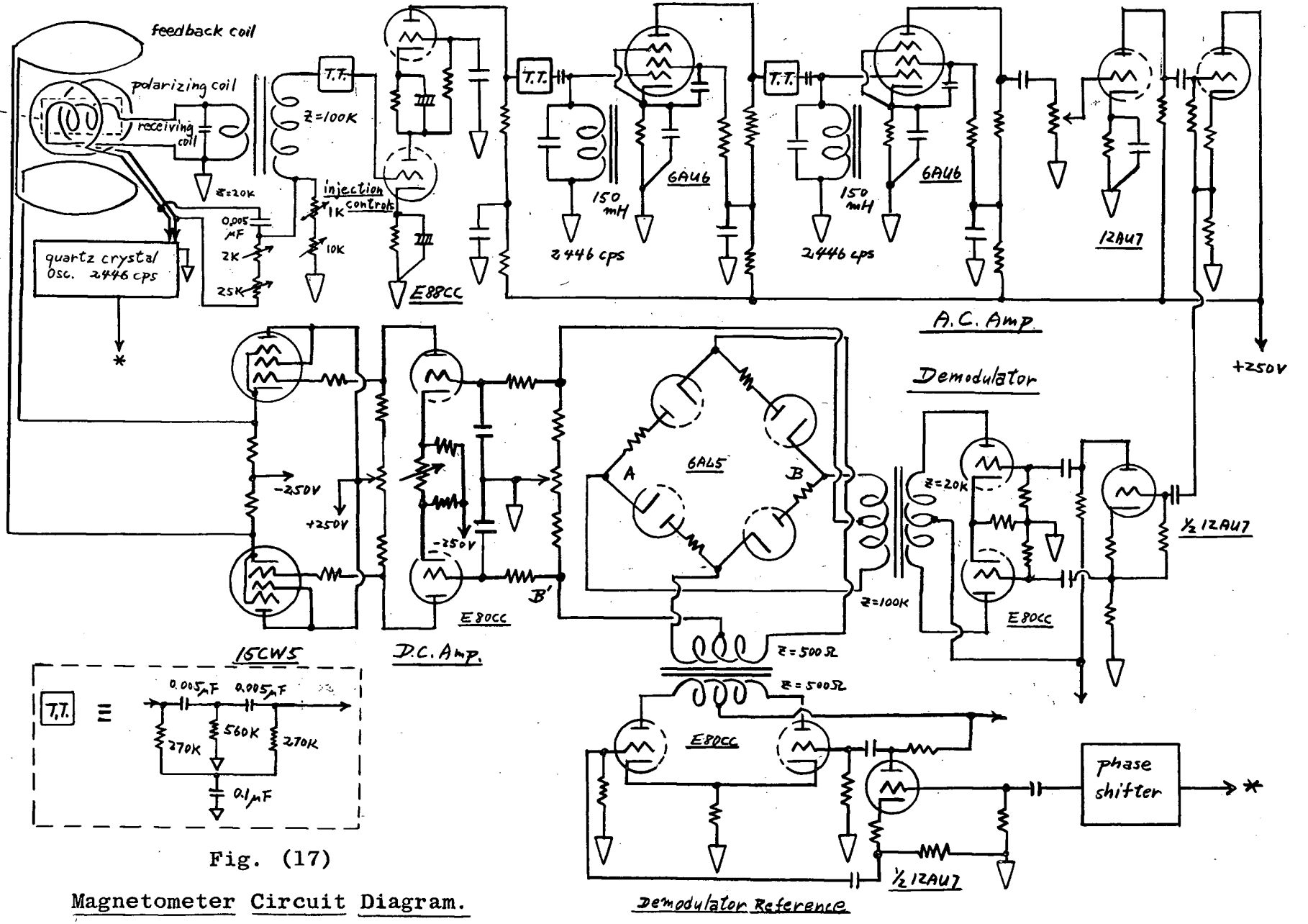

Fig. (17)

Magnetometer Circuit Diagram.

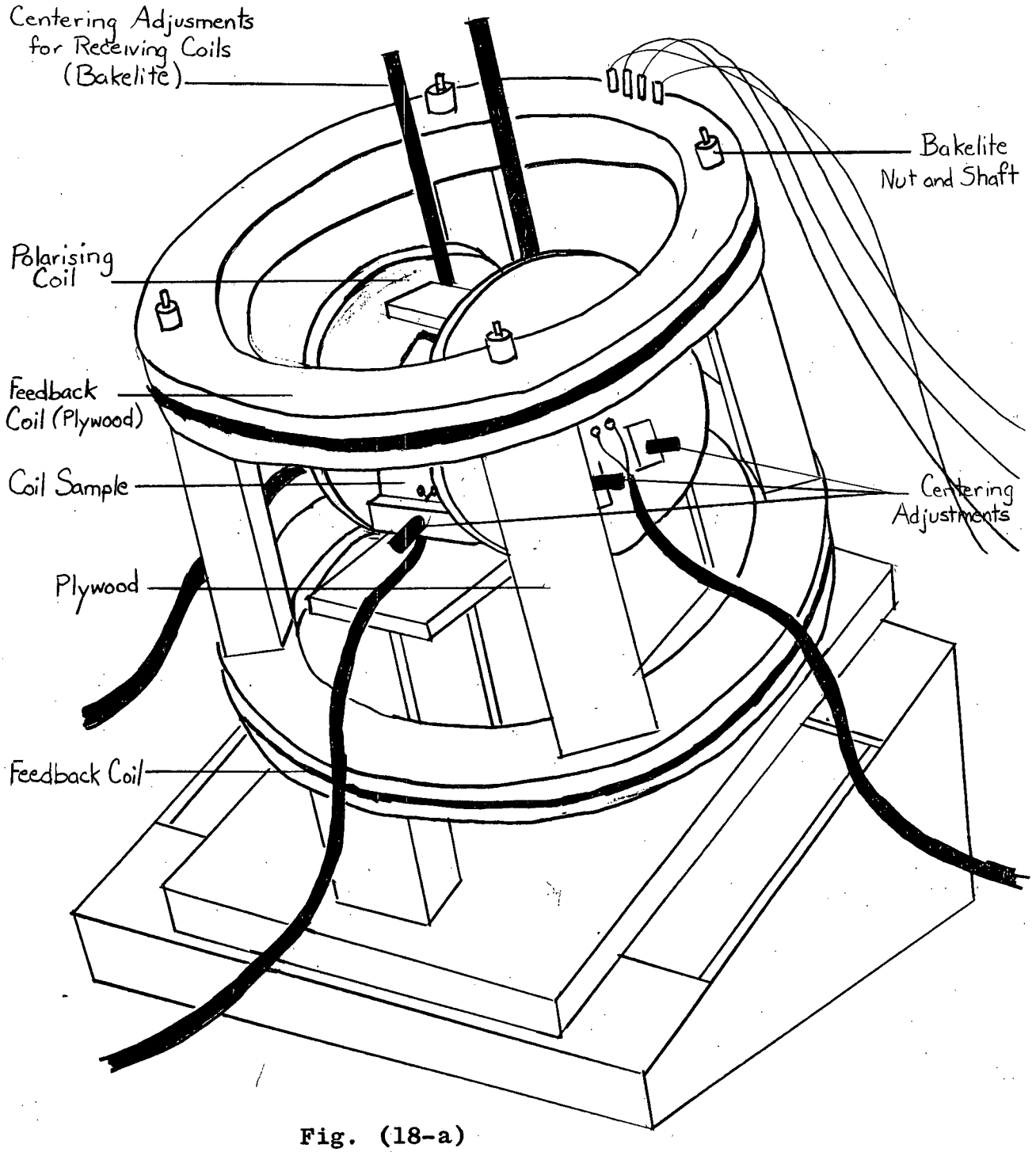

Fig. (18-a)

Crossed Coil System.

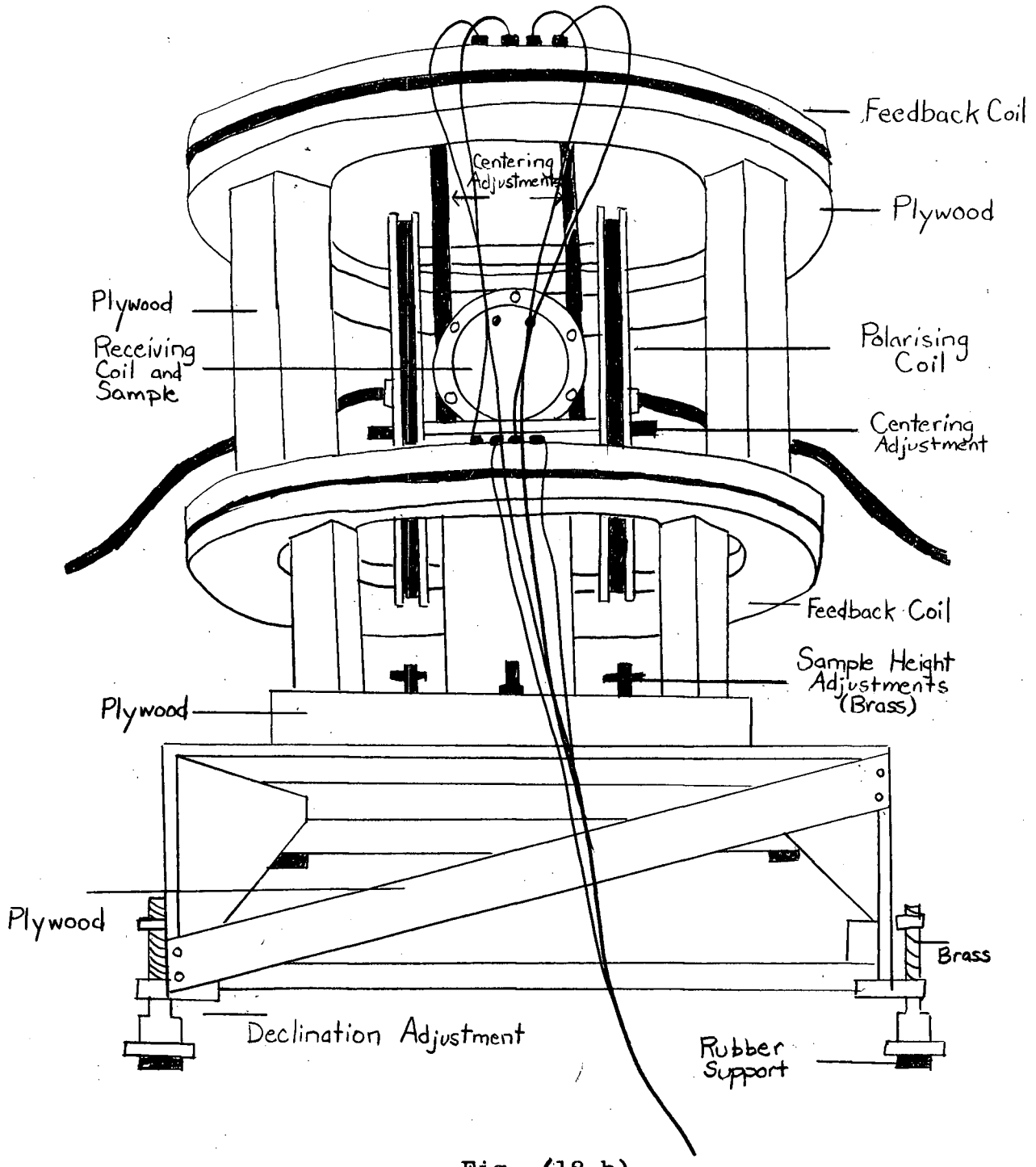

Fig. (18-b)

Crossed Coil System.

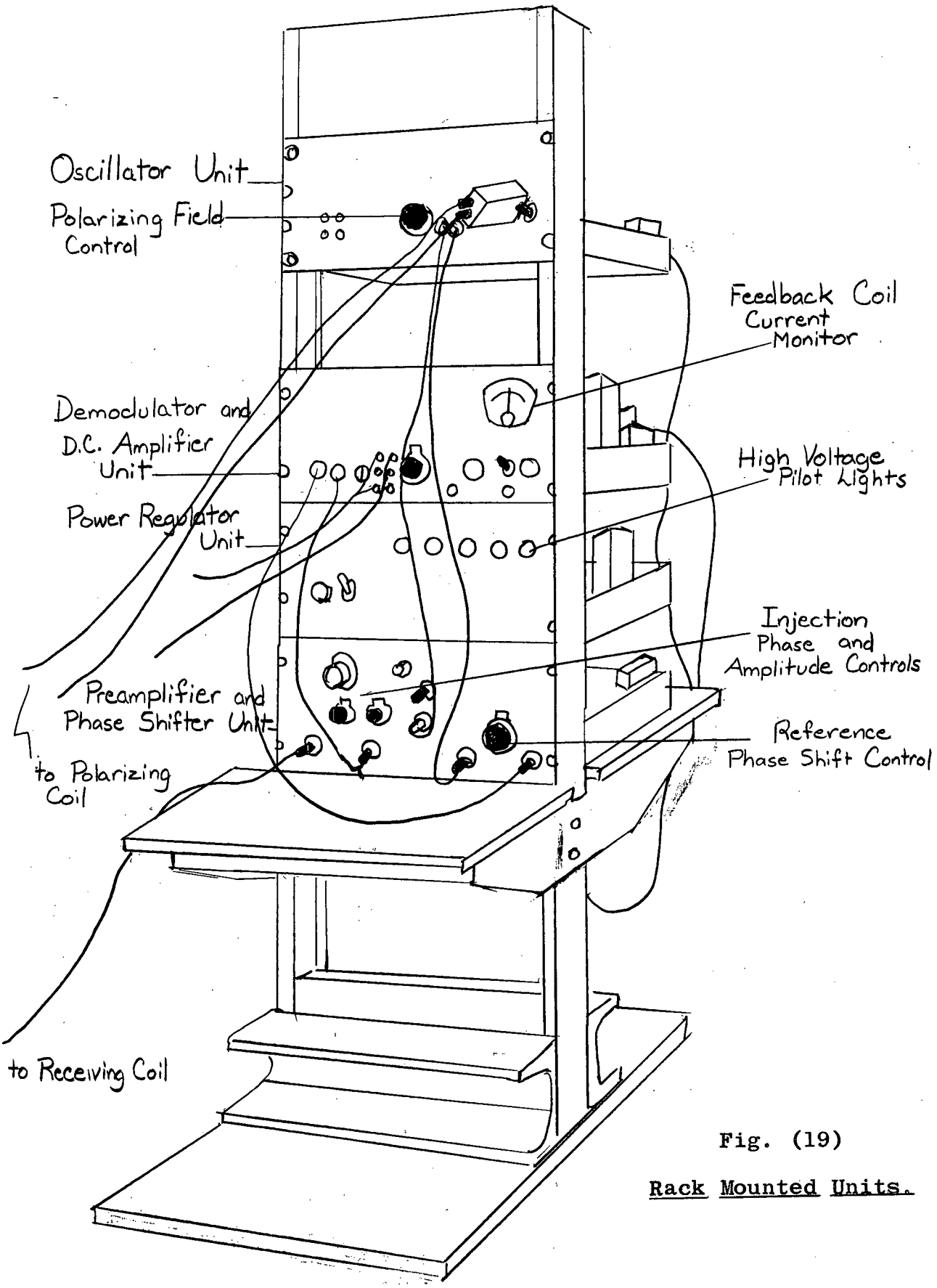

Fig. (19)

Rack Mounted Units.

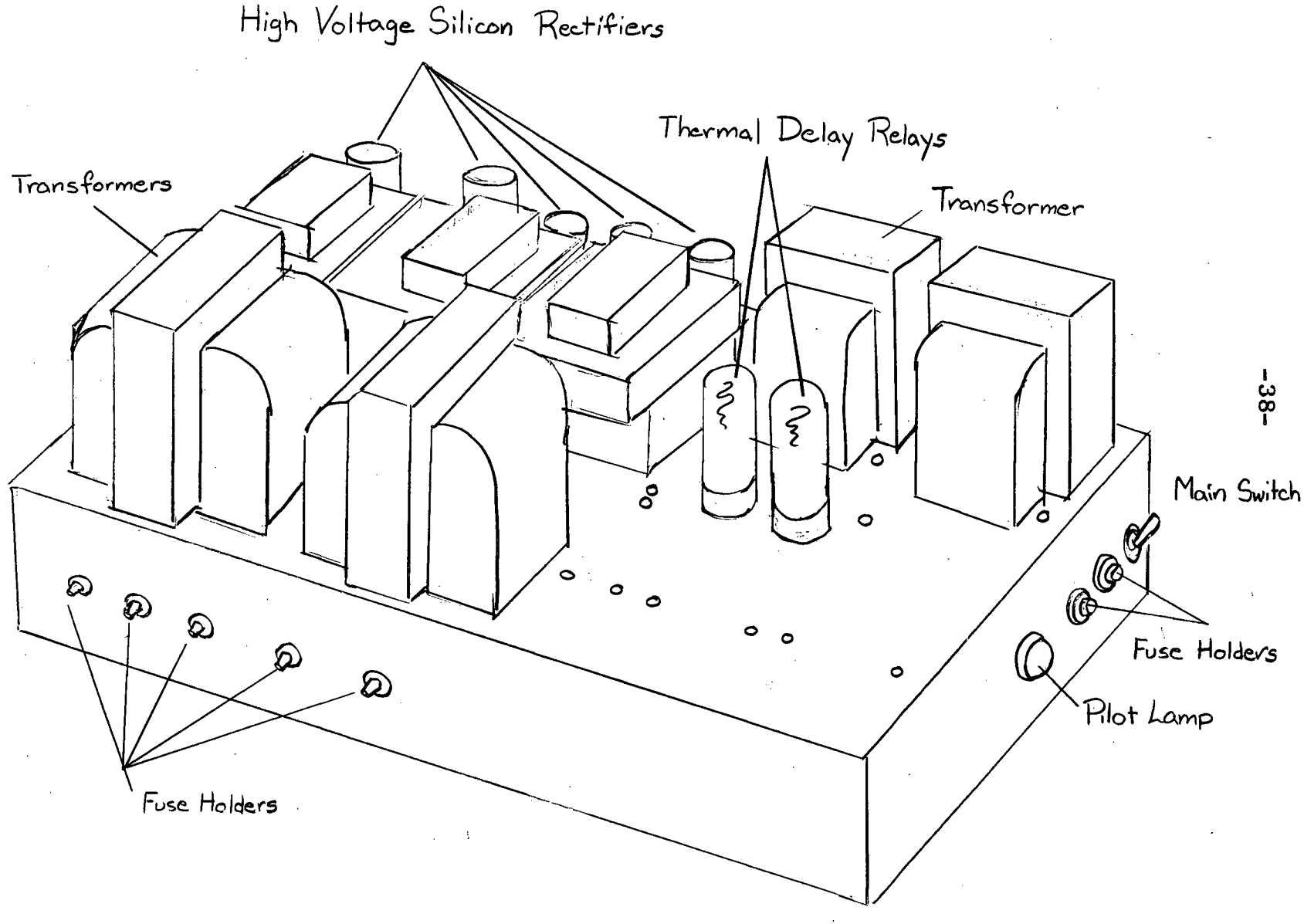

Fig. (20-a)

Transformer Unit.

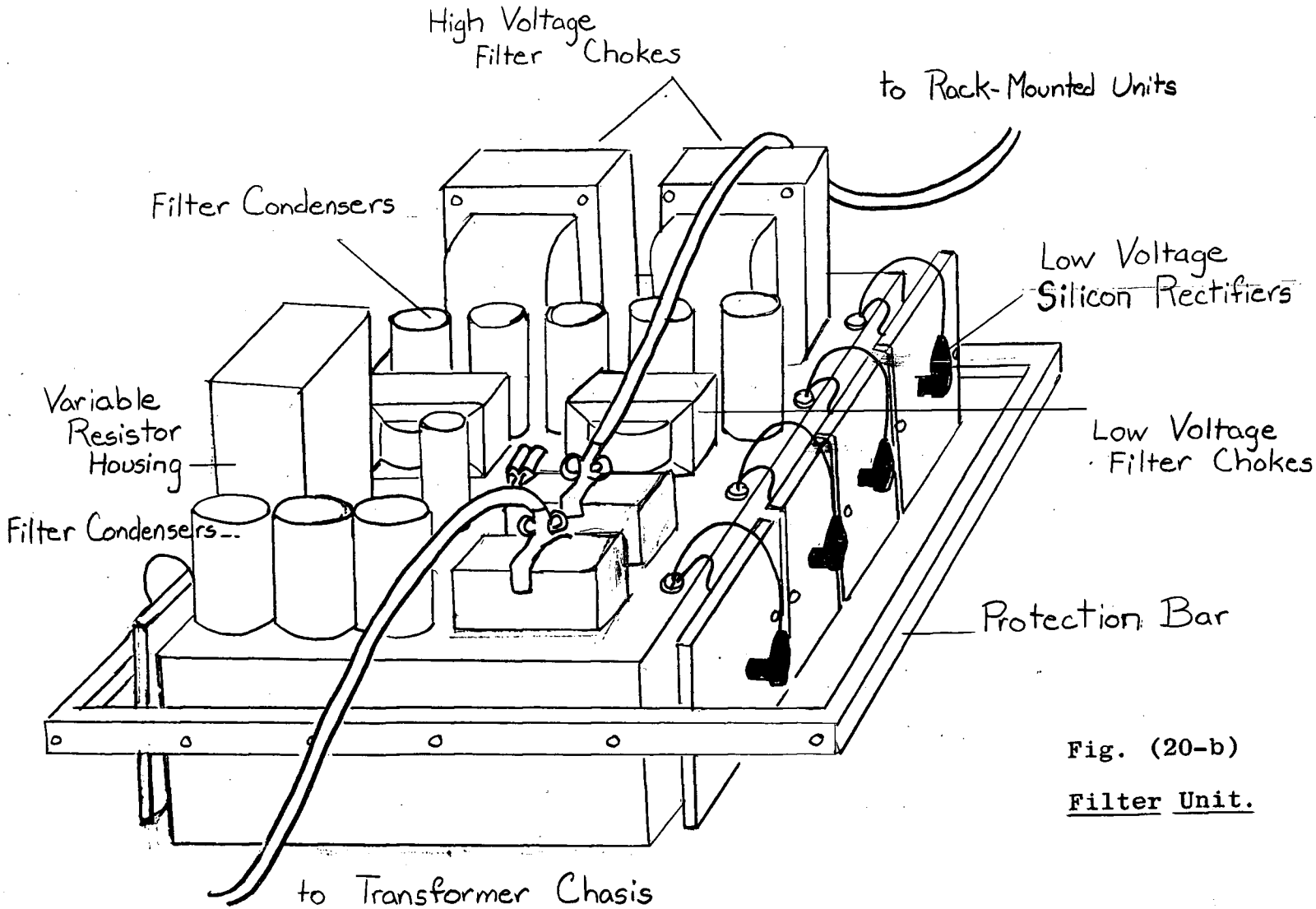

Fig. (20-b)

Filter Unit.

sensitive detector, A.C. amplifier and D.C. amplifier, interactions among the sections are prevented.

2.2 Polarizing Coil System

An oven stabilized quartz crystal oscillator of frequency 2446 cps is employed for the generation of the polarizing magnetic field $\overline{H}_p$. The frequency stability is better than one part in 10^6 and an additional filter is included to reduce harmonics. The temperature control of the oven is accomplished by a transistorised servo system which provides a smooth control of temperature and eliminates the switching noise generated by conventional bimetallic controls.

The polarizing coil is a low impedance system in order to achieve good geometrical symmetry. It is of the Helmholtz configuration employing two ring like coils of mean diameter 58.5 cm. Thirty-four turns of No. 14 wire are wound in two layers. The sensitivity of the coil is given by

$$\frac{H}{i} = \frac{32}{5\sqrt{5}} \frac{1}{10} \frac{N}{r} = 1.04 \text{ (gauss/ampere)} \qquad (2\text{-}1)$$

where H = field intensity at the center of the coil system in gauss

r = radius in cm

n = number of turns

and i = current in amperes.

The inhomogeneity of the field across the sample is

considered negligible in practice.

The coil system is oriented so that the planes of the coils are contained in the geomagnetic meridian. To cancel the leakage of the polarizing field a phase shift network with an amplitude control is employed to inject a small signal into the A.C. amplifier from the quartz crystal oscillator.

2.3 Receiving Coil and A.C. Amplifier

The receiving coil is also of low impedance in order to achieve good geometrical symmetry. The mean diameter is 18.5 cm and the length 23 cm. It has a total of 240 windings in two layers using 49 conductor "Litz" wire. As a Faraday shield an extra layer of No. 12 enamel covered solid wire is wound with only one end connected to ground. The inductance of the coil is approximately 40 millihenries and is tuned to 2446 cps by condensers connected across the coil. The coil bobbin is constructed of plastic and fiberglass and is also a watertight container. Therefore, the water sample is very closely coupled to the receiver coil. The volume of the sample is 5.8 liters, which is large compared to usual nuclear magnetic resonance experiments. The receiving coil is oriented so that the coil axis is contained in the geomagnetic meridian and intersects the main geomagnetic field at right angles. A mechanical device is provided for adjusting the receiving coil position in order to have minimum

coupling with the polarizing coil system.

The first stage amplifier is a cascode circuit employing a type E88CC special quality vacuum tube in order to achieve a good signal to noise ratio. The second and third stages have high Q factor parallel resonance circuits with resonance frequency at 2446 cps. "Twin T" rejection filters are inserted to prevent the 60 cps noise from "ringing" the parallel resonance circuits. Most of the extraneous noise is greatly attenuated by the two stages. The following stages up to the demodulator are resistor and capacitor coupled.

2.4 Demodulator

The demodulator receives the carrier signal and reference signal through identical pushpull amplifiers with transformers. The circuit employed is known as the "Ring Demodulator"[16] and operates as a full wave demodulator. For each half cycle of the reference the two pairs of diodes on the left and on the right conduct alternately. Therefore, point A or B is set to potential B′ each half cycle, completing the switching action described in Chapter I, Section 6. The phase shifter varies the phase of the reference signal so that the u-mode signal is selected.

2.5 D.C. Amplifier and Feedback Coil System

The D.C. amplifier consists of difference amplifiers[17] with high common mode rejection to minimize the effects of

power supply noise. The output tubes have high transconductance and can deliver a maximum of 25 mA to a low resistance load.

The feedback coil is a large Helmholtz coil system with a mean radius of 60.5 cm and 34 turns of enamel covered No. 14 wire in two layers on each coil. The sensitivity of the coil is

$$\frac{H}{i} = 0.505 \text{ gauss/ampere}$$

Other windings are also provided on the coil for various purposes which will be mentioned in Chapter IV. The orientation of the coil is such that its axis coincides with the main geomagnetic field.

CHAPTER III

THEORETICAL PERFORMANCE

3.1 Approximations and Component of Geomagnetic Variations Measured

The configuration of the magnetometer coil system is shown in Fig. (21). The expression for the u-mode signal which is detected is

$$v_1(t) = \frac{1}{c} \; 4\pi NAw_r \; \frac{H_1 M(\gamma T_2^*)^2 \{ F(t)-H_r \} \cos w_r t}{1 + (\gamma H_1)^2 T_1 T_2^* + (\gamma T_2^*)^2 \{F(t) - H_r\}^2} \qquad (3\text{-}1)$$

where it is assumed that the variation of $\overline{F}$ is in the direction of the z axis. In practice this will not be the case and it must be shown that equation (3-1) is a good approximation for the u-mode signal actually observed. The value of the main field at the University of British Columbia, Vancouver, Canada, is approximately 0.5 gauss and the maximum variation of the geomagnetic field $\overline{F}$, rarely exceeds 200 γ at the site. Therefore, the maximum angle α between the initial value $\overline{H}_r$ and the final value $\overline{F}'$ of $\overline{F}$ is of the order

$$\alpha = \text{arc sin} \frac{200}{0.5 \times 10^{-5}} = 4 \times 10^{-3}$$

Fig. (22) shows the relative positions of the macroscopic

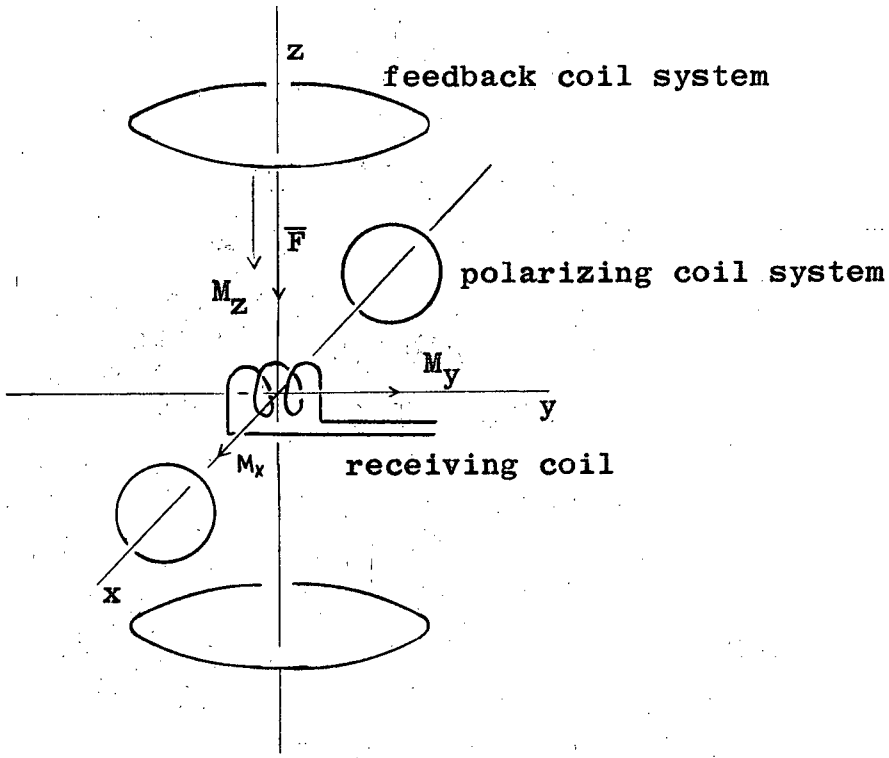

Fig. (21)

Magnetometer Coil System.

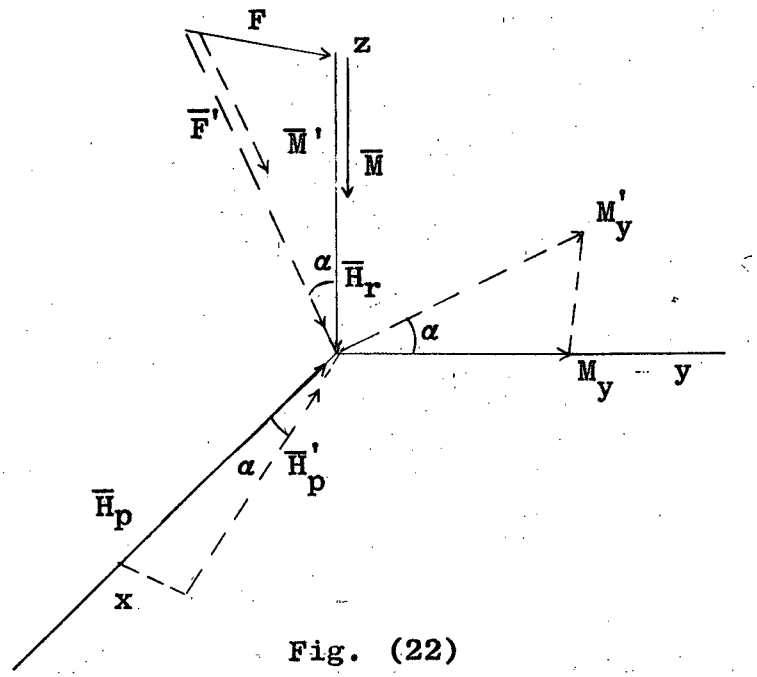

Fig. (22)

Relative Positions of Magnetic Vectors.

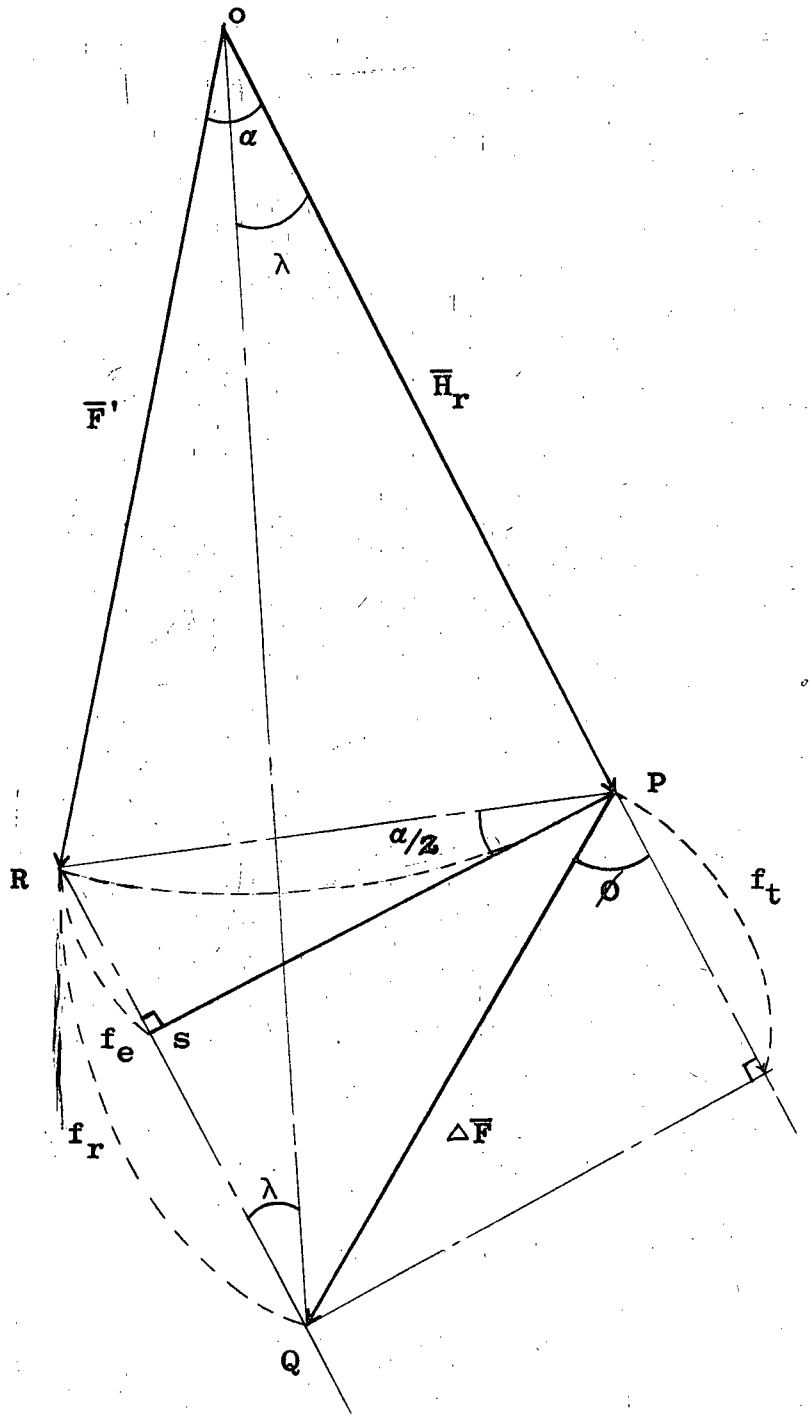

Fig. (23)

Magnitude of Error f_e of Recorded Component f_r.

magnetic moment $\overline{M}$, the polarizing magnetic field $\overline{H}_p = 2\overline{H}_1 \cos w_r t$, and the geomagnetic field $\overline{F}$, before and after the change $\triangle\overline{F} = \overline{F}(t)-\overline{H}_r$. The receiver coil is sensitive only to the components of $\overline{M}$ along the y axis. Therefore, the magnitude of the signal after the variation $\triangle\overline{F}$ is,

$$v_1(t) = \frac{1}{c}\, 4\pi NAw_r \, \frac{H_1 M(\cos^2 \alpha)(\gamma T_2^*)^2 \left\{F'(t)-H_r\right\} \cos w_r t}{1 + (\gamma H_1 \cos \alpha)^2 T_1 T_2^* + (\gamma T_2^*)^2 \left\{F'(t)-H_r\right\}^2}$$

Since $\alpha \approx 4 \times 10^{-3}$ is the largest angle expected,

$$\cos^2 \alpha \approx 1$$

and the equation is a good approximation.

The negative feedback is applied along the axis of the feedback coil system which is parallel to the main geomagnetic field and the magnitude of the field is maintained at the resonance value H_r. The relations between the initial main field $\overline{H}_r$, the final main field $\overline{F}'$, the variation $\triangle\overline{F}$, and the feedback f_r, are shown in Fig. (23), on a greatly exaggerated scale.

From the preceding discussion it is apparent that $F' \approx H_r$. The symbol f_t is the actual component of $\triangle\overline{F}$ along the main field, and the recorded signal f_r contains an error f_e such that

$$f_t = f_r - f_e \,.$$

Referring to Fig. (23), the following relations are apparent:

$$f_e = (R\ S) = (P\ S) \tan \alpha/2 = \Delta F \sin \phi \tan \alpha/2$$

$$\angle O\ R\ Q = 180^\circ - \alpha$$

$$(O\ Q) \sin \lambda = \Delta F \sin \phi$$

and $$(O\ Q) \sin \lambda = F' \sin \alpha = H_r \sin \alpha \ .$$

Therefore,

$$\sin \alpha = \frac{\Delta F \sin \phi}{H_r} \ .$$

For small α (in our case $\alpha \approx 4 \times 10^{-3}$)

$$\sin \alpha \approx \alpha$$

and $$\tan \alpha/2 \approx \alpha/2 \ .$$

It follows that

$$\tan \alpha/2 \approx \alpha/2 \approx \frac{\Delta F \sin \phi}{2\ H_r}$$

and

$$f_e = \frac{\Delta F^2 \sin^2 \phi}{2\ H_r} \ .$$

The maximum recorded error expected is then, for

$$\Delta F = 200\ \gamma$$

$$\phi = 90^\circ$$

$$H_r = 5 \times 10^4\ \gamma$$

$$f_e = \frac{200^2}{2 \times 5 \times 10^4}\ \gamma = 0.2\ \gamma \ .$$

Thus, the error is of reasonable magnitude and the component f_r that is recorded is a good representation of

the component of $\Delta \overline{F}$ along the main geomagnetic field.

3.2 Sensitivity of the Receiving Coil

The u-mode signal as a function of $\Delta F = F(t) - H_r$ is

$$S_u = \frac{H_1 M(\gamma T_2^*)^2 \Delta F \cos w_r t}{1 + (\gamma H_1)^2 T_1 T_2^* + (\gamma T_2^*)^2 (\Delta F)^2} \quad .$$

The first derivative of S_u with respect to ΔF is

$$\frac{dS_u}{d(\Delta F)} = S_u^* = \frac{\left\{1-(\gamma T_2^*)^2(\Delta F)^2 + (\gamma H_1)^2 T_1 T_2^*\right\} H_1 M(\gamma T_2^*)^2 \cos w_r t}{\left\{1 + (\gamma H_1)^2 T_1 T_2^* + (\gamma T_2^*)^2 (\Delta F)^2\right\}^2}$$

The graphical forms of the amplitudes of S_u and S_u^* are given in Fig. (24). The maxima and minima of the amplitude of S_u are

$$(S_u)_{max} = \pm\tfrac{1}{2} \frac{H_1 M \gamma T_2^*}{\left\{1+(\gamma H_1)^2 T_1 T_2^*\right\}^{\frac{1}{2}}}$$

and occurs when

$$F = (\Delta F)_{max} = \pm \frac{1}{\gamma T_2^*} \left\{1 + (\gamma H_1)^2 T_1 T_2^*\right\}^{\frac{1}{2}}$$

The maximum amplitude of S_u^* occurs at $\Delta F = 0$ and is given by

$$(S_u^*)_{max} = \frac{H_1 M(\gamma T_2^*)^2}{1 + (\gamma H_1)^2 T_1 T_2^*} \quad .$$

Since the negative feedback attempts to maintain the resonance

condition, $\Delta F = 0$, in order to have high sensitivity the amplitude of S_u^* at the origin, $(S_u^*)_{max}$ must be large. The graph of $(S_u^*)_{max}$ as a function of H_1 is shown in Fig. (25). The constants that determine the value of $(S_u^*)_{max}$ are T_1, T_2^* and H_1. The relaxation time constants are fixed for a given sample. Therefore, H_1 must be varied to obtain the optimum sensitivity. It is readily shown that $(S_u^*)_{max}$ reaches a maximum value when

$$H_1 = \frac{1}{\gamma}\sqrt{\frac{1}{T_1 T_2^*}} \qquad (3\text{-}1)$$

The magnitude of the signal across the receiving coil is

$$v_1(t) = \frac{1}{c}\, 4\pi\, NA\, w_r \frac{H_1 M(\gamma T_2^*)^2 \Delta F \cos w_r t}{1 + (\gamma H_1)^2 T_1 T_2^* + (\gamma T_2^*)^2 (\Delta F)^2}$$

For very small ΔF, $v_1(t)$ can be expanded in terms of a Taylor Series and the following approximation for $v_1(t)$ is obtained,

$$v_1(t) \approx \frac{1}{c}\, 4\pi\, NA\, w_r \frac{H_1 M(\gamma T_2^*)^2}{1 + (\gamma H_1)^2 T_1 T_2^*}\, \Delta F \cos w_r t \ .$$

This approximation is reasonable because the negative feedback will keep the variation of ΔF within a very small range. The sensitivity of the receiving coil is then

$$\frac{v_1(t)}{\Delta F} = \frac{1}{c}\, 4\pi NA\, w_r \frac{H_1 M(\gamma T_2^*)^2}{1 + (\gamma H_1)^2 T_1 T_2^*} \qquad (3\text{-}2)$$

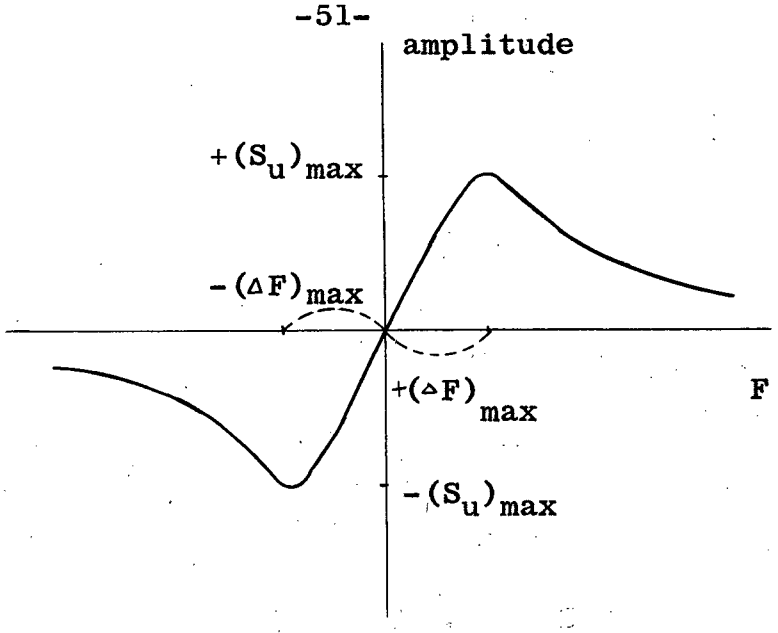

amplitude of u-mode signal

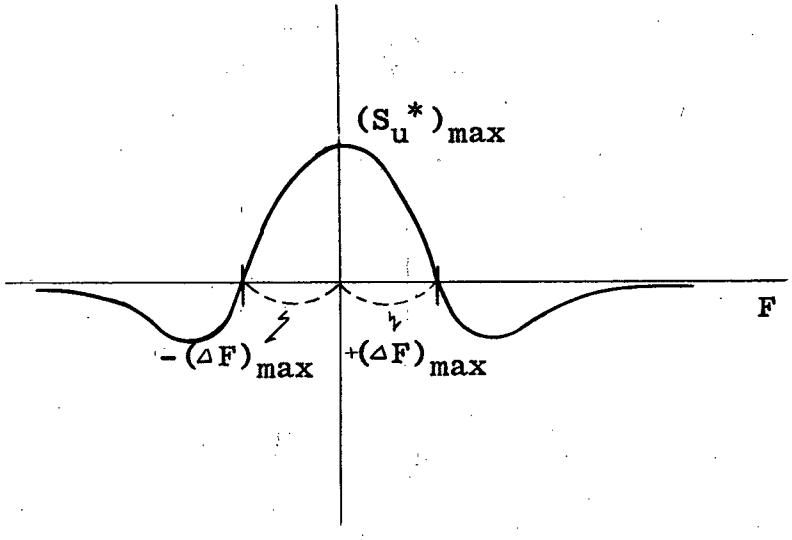

Variation of slope of (S_u^*)

Fig. (24)

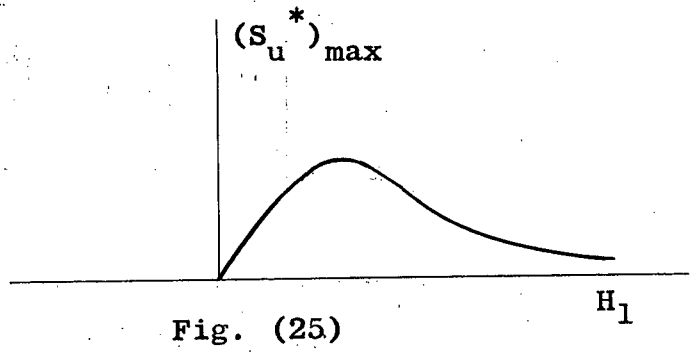

Fig. (25)

Variation of $(S_u^*)_{max}$.

Optimum sensitivity is obtained when H_1 satisfies equation (3-1), and equation (3-2) then becomes

$$\frac{v_1(t)}{\Delta F} = \frac{1}{c}\, 4\pi\, NA\, w_r\, M\, \frac{1}{2}\, \gamma\, T_2^* \sqrt{\frac{T_2^*}{T_1}}$$

For ordinary distilled water, the relaxation times T_1 and T_2^* are approximately 2.8 seconds[18], and the optimum sensitivity is then

$$\frac{v_1(t)}{\Delta F} = \frac{1}{c}\, 4\pi\, NA\, w_r\, XH_r\, C\, \frac{1}{2}\, \gamma\, T_2^* = 2.8 \text{ mV/gauss}$$

where $c = 3 \times 10^{10}$ cm/sec

$N = 240$

$A = 269$ cm^2

$w_r = 2446$ cps

$X = 3.4 \times 10^{-10}$ paramagnetic susceptibility of the hydrogen nuclei in water

$H_r = 0.575$ gauss

$C = 5.8 \times 10^3$ cm^3, the volume of the sample

and $\gamma = 2.675 \times 10^4$/sec gauss.

3.3 System Transfer Function

To determine the characteristic of the magnetometer it is necessary to determine its transfer function. A simplified block diagram of the nuclear magnetic resonance phenomenon which acts as the error detector and modulator

is shown in Fig. (26). The transfer function of the modulator is obtained from the sensitivity of the receiving coil, where the input is the geomagnetic variation $\triangle F$ and the output is the voltage $v_1(t)$ across the receiving coil. From the preceding section the sensitivity of the coil is given by

$$v_1(t) = K_1 \, \Delta F(t)$$

where

$$K_1 = \frac{1}{c} \, 4\pi NAw_r \, \frac{H_1 M(\gamma T_2^*)^2}{1+(\gamma H_1)^2 T_1 T_2^*} \quad .$$

It follows immediately that the transfer function is

$$\frac{L\left\{v_1(t)\right\}}{L\left\{\Delta F(t)\right\}} = K_1 \quad .$$

The A.C. amplifier has a constant gain factor K_2 where

$$K_2 = \frac{L\left\{v_2(t)\right\}}{L\left\{v_1(t)\right\}} = \frac{V_2(s)}{V_1(s)}$$

and $v_2(t)$ is the amplitude of the output voltage of the A.C. amplifier.

The demodulator has a low pass filter, as shown in Fig. (27), which contributes the dominating time constant of the system. Referring to Fig. (27), we have as the input voltage

$$K_3 V_2(s) = I(s) \left(2R_3 + \frac{2}{sC_3} \right)$$

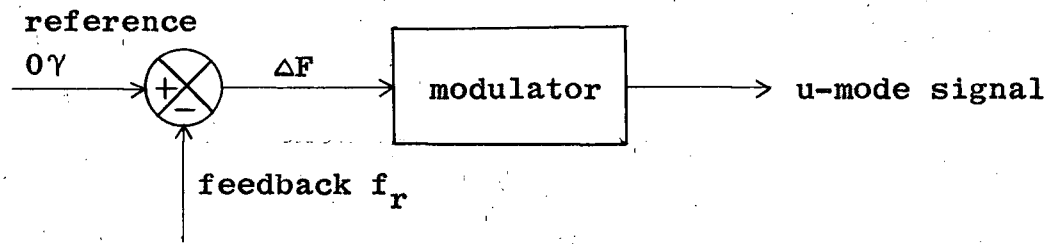

Fig. (26)

Simplified Block Diagram of Nuclear Magnetic Resonance Phenomenon.

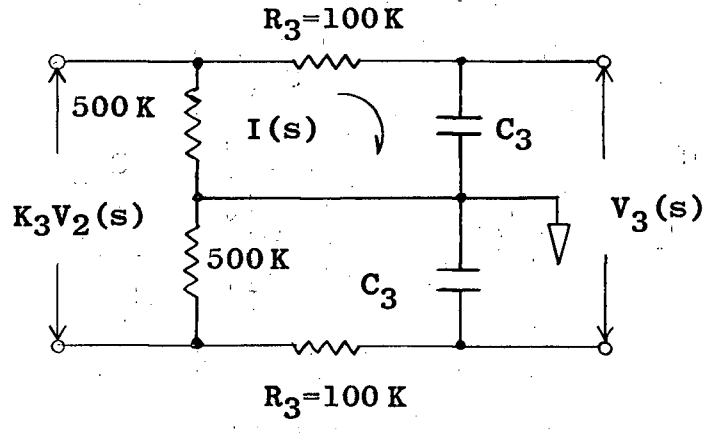

Fig. (27)

Demodulator Filter.

and as the output voltage

$$V_3(s) = I(s)\frac{2}{sC_3} \quad .$$

The symbol K_3 is the gain constant of the switching section of the demodulator. The transfer function is then,

$$\frac{V_3(s)}{V_2(s)} = K_3 \frac{1}{sT_3 + 1}$$

where

$$T_3 = R_3C_3 \quad .$$

The D.C. amplifier has a constant gain factor K_4 where

$$K_4 = \frac{I(s)}{V_3(s)}$$

and $L^{-1}\{I(s)\}$ is the output current which is to be recorded.

The forward transfer function is then,

$$K_fG(s) = \frac{V_1(s)}{L\{\Delta F\}} \cdot \frac{V_2(s)}{V_1(s)} \cdot \frac{V_3(s)}{V_2(s)} \cdot \frac{I(s)}{V_3(s)} = K_1K_2K_3K_4 \frac{1}{sT_3+1} \qquad (3\text{-}3)$$

where $K_f = K_1K_2K_3K_4$.

Using 2.8 mV/gauss as the sensitivity of the receiving coil and by determining the gain of the amplifiers experimentally K_f is found to be approximately equal to 2.8 mA/γ. The time constant T_3 is switched in steps over the values 0.001, 0.01, 0.05, 0.2, 0.4 and 0.8 seconds in order to vary the frequency

response of the system.

The feedback transfer function is a constant K_5 given by the feedback Helmholtz coil system, where the input is the current I(s) and the output is a magnetic field $f_r(s)$. K_5 is calculated to be

$$K_5 = 0.505 \text{ gauss/amp} \quad . \tag{3-4}$$

From the forward transfer function (3-3) and feedback transfer function (3-4) the overall feedback system transfer function Y(s) is obtained. From feedback system theory we have

$$Y(s) = \frac{K_f G(s)}{1 + K_5 K_f G(s)} = \frac{K_f \dfrac{1}{sT_3+1}}{1 + K_5 K_f \dfrac{1}{sT_3+1}}$$

It follows that

$$Y(s) = \frac{K}{sT + 1} \tag{3-5}$$

where $K = \dfrac{K_f}{1+K_f K_5}$ and $T = \dfrac{T_3}{1+K_f K_5}$.

Since $K_f = 2.8$ mA/γ and $K_5 = 0.505$ gauss/amp, for $T_3 = 0.8$ sec we have,

$$Y(s) = \frac{20 \ \mu A/\gamma}{s \ 5.6 \times 10^{-3} \text{sec} + 1} \quad .$$

3.4 Stability

The closed loop transfer function or the system transfer function of the magnetometer is given by

$$Y(s) = \frac{K}{sT+1} \quad . \tag{3-5}$$

The stability of the response of the system to transients is revealed by the inverse Laplace transform of Y(s), viz:

$$L^{-1}\left\{ Y(s) \right\} = K \frac{1}{T} \exp\left(-\frac{t}{T}\right) .$$

Since T is positive, as t increases $L^{-1}\left\{ Y(s) \right\}$ tends to zero. Therefore, the system is stable.

To determine the degree of stability the block diagram of the magnetometer is redrawn in Fig. (28) to show the feedback magnetic field f_r as the output.

The loop transfer function of the magnetometer is then

$$K_o G_o(s) = \frac{K_1 K_2 K_3 K_4 K_5}{sT_3 + 1} \quad .$$

The decibel gain amplitude and phase angle, plotted against logarithmic frequency, generally known as the Bode Diagram, of $K_o G_o(s)$ is given in Fig. (29). Reading from the Bode Diagram, the phase margin is at least 90° for all frequencies and there is no question of instability.

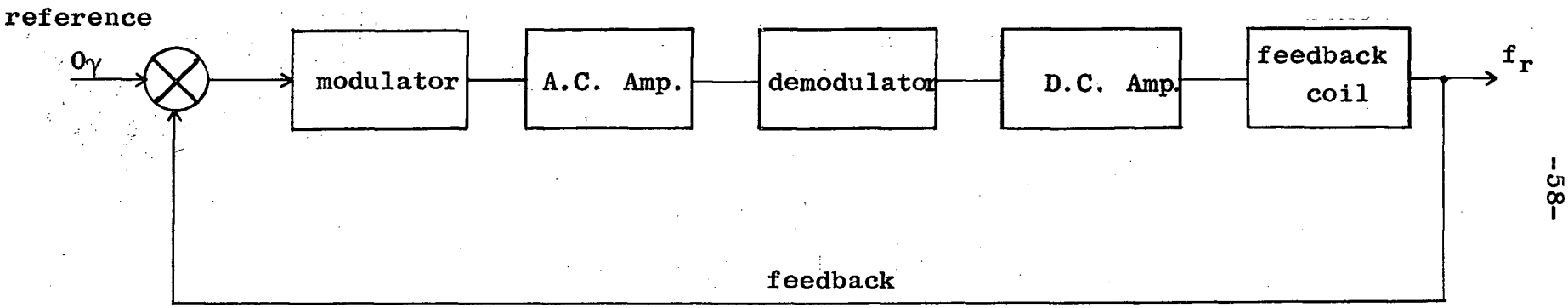

Fig. (28)

Magnetometer Block Diagram with Recorded Component as Output.

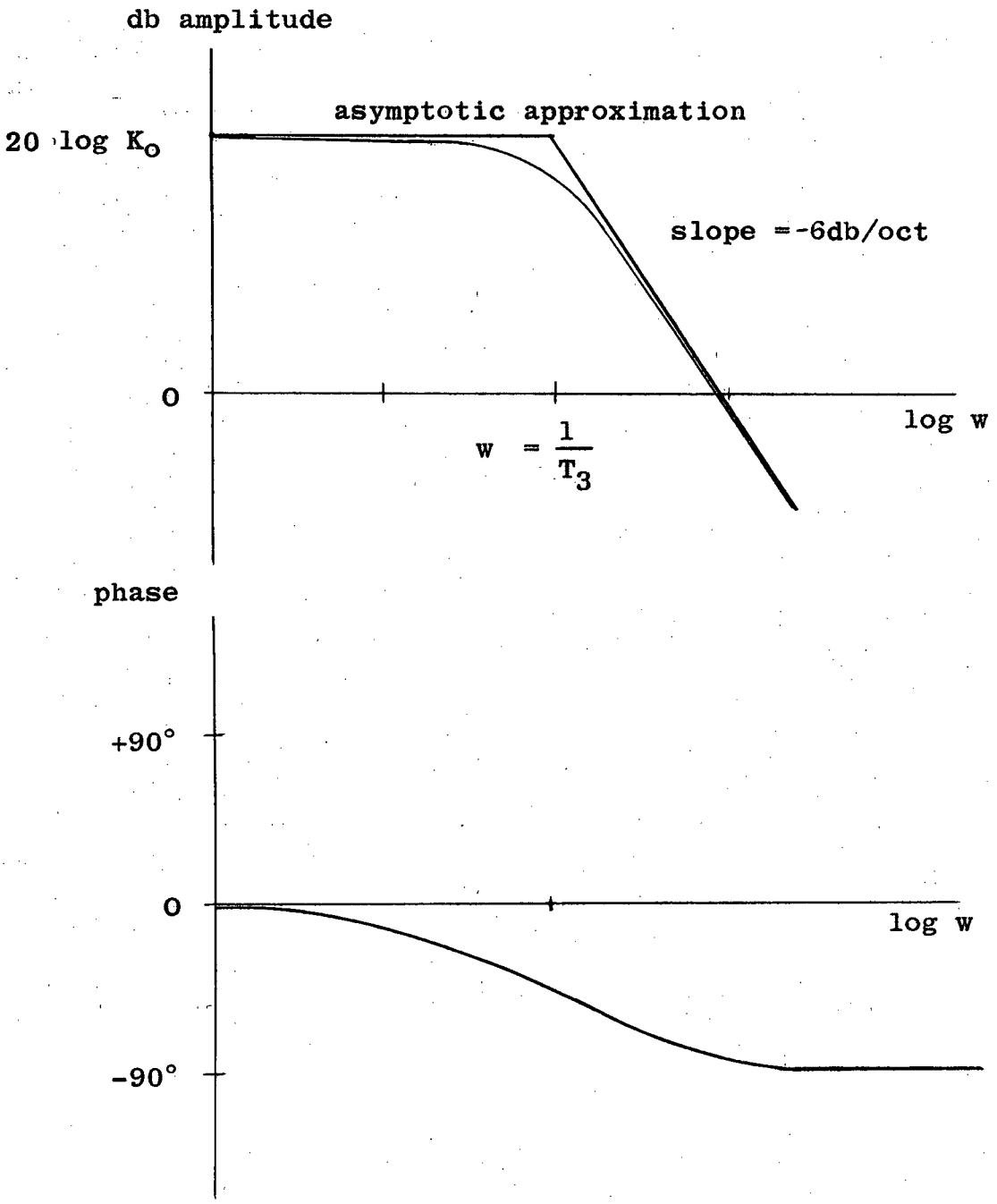

Fig. (29)

Bode Diagrams of the Magnetometer.

3.5 Response to Some Input Functions

In order to obtain information to compare the theoretical and operational performance, the response to some input functions of interest are computed below.

Sinusoidal Function :

$$I(s) = L\left\{\sin Wt\right\} \cdot Y(s) = \frac{W}{s^2+W^2} \cdot \frac{K}{sT+1}$$

Referring to tables of Laplace transforms[19][20], we obtain

$$i(t) = L^{-1}\left\{I(s)\right\} = \frac{KW}{T} \cdot \frac{1}{\frac{1}{T^2}+W^2} \cdot \left\{\exp\left(-\frac{t}{T}\right)+\frac{1}{W}\sqrt{\frac{1}{T^2}+W^2}\sin(wt-\Theta)\right\}$$

where $\Theta = \tan^{-1} WT$.

The steady state response, where t is large, is

$$i(t) = \frac{K}{\sqrt{1+(WT)^2}} \sin\ (Wt - \Theta) \ .$$

Ramp Function :

A ramp function is given by

$$r(t) = \begin{cases} 0 & t < 0 \\ At & t \geq 0 \end{cases}$$

where A is a constant, and

$$L\left\{r(t)\right\} = \frac{A}{s^2} \ .$$

Then

$$I(s) = \frac{A}{s^2} \cdot Y(s) = \frac{AK}{T} \ \frac{1}{s^2} \ \frac{1}{s+\frac{1}{T}} \ .$$

Applying the convolution theorem, we obtain

$$i(t) = L^{-1}\left\{ I(s)\right\} = AK\left\{ T\exp(-t/T) + t - T \right\}$$

For large t, we have

$$i(t) = AK\ (t-T)\ . \qquad (3\text{-}6)$$

Step Function:

A step function is defined as

$$u(t) = \begin{cases} 0 & t < 0 \\ A & t > 0 \end{cases}$$

where A is a constant, and $L\left\{u(t)\right\} = \frac{A}{s}$.

Obviously the condition given by equation (1-6) in Chapter I, Section 3,

$$\left|\frac{dF}{dt}\right| \ll \gamma\ H_1^2$$

for the validity of the expression of the macroscopic magnetic moment $M_y = -(u \sin w_r t + v \cos w_r t)$ is not satisfied. However, as a point of interest the response is derived.

$$I(s) = \frac{K}{T}\frac{A}{s}\frac{1}{(s+\frac{1}{T})} = KA\left\{\frac{1}{s} - \frac{1}{s+\frac{1}{T}}\right\}$$

$$i(t) = L^{-1}\left\{I(s)\right\} = KA\ \left\{\frac{u(t)}{A} - \exp\ (-\frac{t}{T})\right\}.$$

For large t,

$$i(t) = K\, u(t) \quad .$$

3.6 Sensitivity of the Magnetometer

Provided that the variations ΔF take place within the limits of the condition expressed by equation (1-6), the sensitivity of the system is given by the constant factor of the closed loop transfer function Y(s). Therefore, the expected sensitivity is,

$$K = 20\ \mu A/\gamma \quad .$$

3.7 Steady State Error

One method of expressing the quality of performance of a feedback system is to give the magnitude of the steady state error of the system to a ramp function input. This method is well suited for the magnetometer since the geomagnetic variations of interest are below 20 c.p.s. and step function inputs are unlikely to occur. Consider the response to the ramp function input given by,

$$F(t) = \begin{cases} 0 & t < 0 \\ 2 \times 10^3\ (\gamma/\text{sec})t & t \geq 0 \end{cases}$$

The choice is based on the maximum frequency of interest, 20 c.p.s., and the maximum amplitude of the expected variation which is 200 γ. The steady state error, when t

is large, is obtained from equation (3-6) in the preceding section, i.e.

$$f_r(t) = 2 \times 10^3 \ (\gamma/\text{sec}) \ K_r \ KT = 1.1 \ \gamma \ .$$

The magnitude of the error is negligible, since for t = 1 sec, $F = 2 \times 10^3 \ \gamma$.

3.8 Dynamic Range

The dynamic range of the system will be restricted by the half line width of the u-mode signal given by

$$(\triangle F)_{max} = \frac{1}{\gamma T_2} \left\{ 1 + (\gamma H_1)^2 T_1 T_2^* \right\}^{\frac{1}{2}},$$

and the time constant T of the closed loop transfer function as well as the maximum output current of the D.C. amplifier.

The maximum output current of the D.C. amplifier is 25 mA which produces a magnetic field of magnitude $1.26 \times 10^3 \ \gamma$, which is more than adequate to cover any geomagnetic variations.

The time constant T must be small enough to allow the feedback system to apply the compensating field before the variation exceeds the half line width. If the half line width is exceeded by the variation, the operating point of the error detector will be shifted to the negative slope region of the u-mode curve and the negative feedback will become a positive feedback. The result will be an oscil-

The maximum rate of change expected is of the order 4×10^3 γ/sec, as shown in the previous section, and the largest time constant of the system is $T = 5.6 \times 10^{-3}$ sec. Assuming that the system requires $2T = 11.2 \times 10^{-3}$ sec. to apply sufficient feedback the variation will reach

$$F = 4 \times 10^3 \ (\gamma/\text{sec}) \ 2T = 44.2 \ \gamma \ .$$

At the optimum sensitivity of the receiving coil when

$$H_1 = \frac{1}{\gamma} \sqrt{\frac{1}{T_1 T_2^*}} \ ,$$

we have

$$(\Delta F)_{max} = \pm \frac{2}{\gamma T_2^*} \ ,$$

and for $T_2^* = 2.8$ seconds,

$$(\Delta F)_{max} = \pm 1.87 \ \gamma \ .$$

It appears that the dynamic range is not sufficient for the intended application. If $T_3 = 0.001$ sec is used we have

$$T = 7.1 \times 10^{-6} \text{ sec}$$

and

$$F = 4 \times 10^3 \ (\gamma/\text{sec}) \ 2T = 0.57 \ \gamma.$$

Therefore, it is still possible to satisfy the required dynamic range.

3.9 Response to Very Fast Variations

In Chapter I, section 3, it was mentioned that for the validity of the expression for the macroscopic magnetic moment the condition

$$\left|\frac{dF}{dt}\right| \ll \gamma H_1^2$$

must be satisfied. The order of the maximum rate of change expected is 4×10^3 γ/sec and H_1 for optimum sensitivity of the receiving coil is given by $H_1 = 1.3\ \gamma$. The maximum rate of change is of the order

$$\left|\frac{dF}{dt}\right| = 4 \times 10^3\ \gamma/\text{sec}$$

and

$$\gamma H_1^2 = 2.67 \times 10^4 \times 1.3^2\ \gamma/\text{sec} = 4.51 \times 10^4\ \gamma/\text{sec}.$$

The ratio is approximately 10 to 1 and the condition can be considered as satisfied since the order of the rate of change is a maximum estimation.

3.10 Summary

The theoretical sensitivity of the magnetometer is 20 $\mu A/\gamma$. The dynamic range exceeds 200 γ.

However, the line width and slope at $\Delta F = 0$ of the u-mode signal amplitude will depend on the degree of contamination of the water sample by paramagnetic substances,

such as oxygen molecules, and the inhomogeneity of the geomagnetic field across the sample as well as the quality of the demodulator that is employed. It remains to determine the operational performance of the magnetometer.

CHAPTER IV

OPERATIONAL PERFORMANCE

4.1 u-mode Signal

In order to locate the nuclear magnetic resonance signal the D.C. amplifier is used as a sweep amplifier to provide a slowly varying magnetic field over the range from 0 to 1300 γ in approximately 90 seconds. The sweep signal is generated by a multivibrator. An extra winding of 160 turns on the feedback Helmholtz coil is used to apply a biasing field in order to bring the total magnetic field approximately to the resonance field value H_r, which in our case is 0.573 gauss. The sensitivity of the extra winding is 240 γ/mA. A cathode follower is connected to the demodulator output and an "Esterline Angus" chart recorder is driven by the cathode follower. The necessary circuit conversions are shown in Fig. (30). The nuclear magnetic resonance signal is found by systematically sweeping the total field magnitude over the range from 0.4 gauss to 0.6 gauss in 1000 γ steps, allowing for the overlapping of each sweep.

Initially no signal was observed because of the high 60 c.p.s. noise pickup in spite of the three "Twin T" rejection filters. By enclosing the crossed coil system in a plywood box lined with aluminum sheets, the 60 c.p.s.

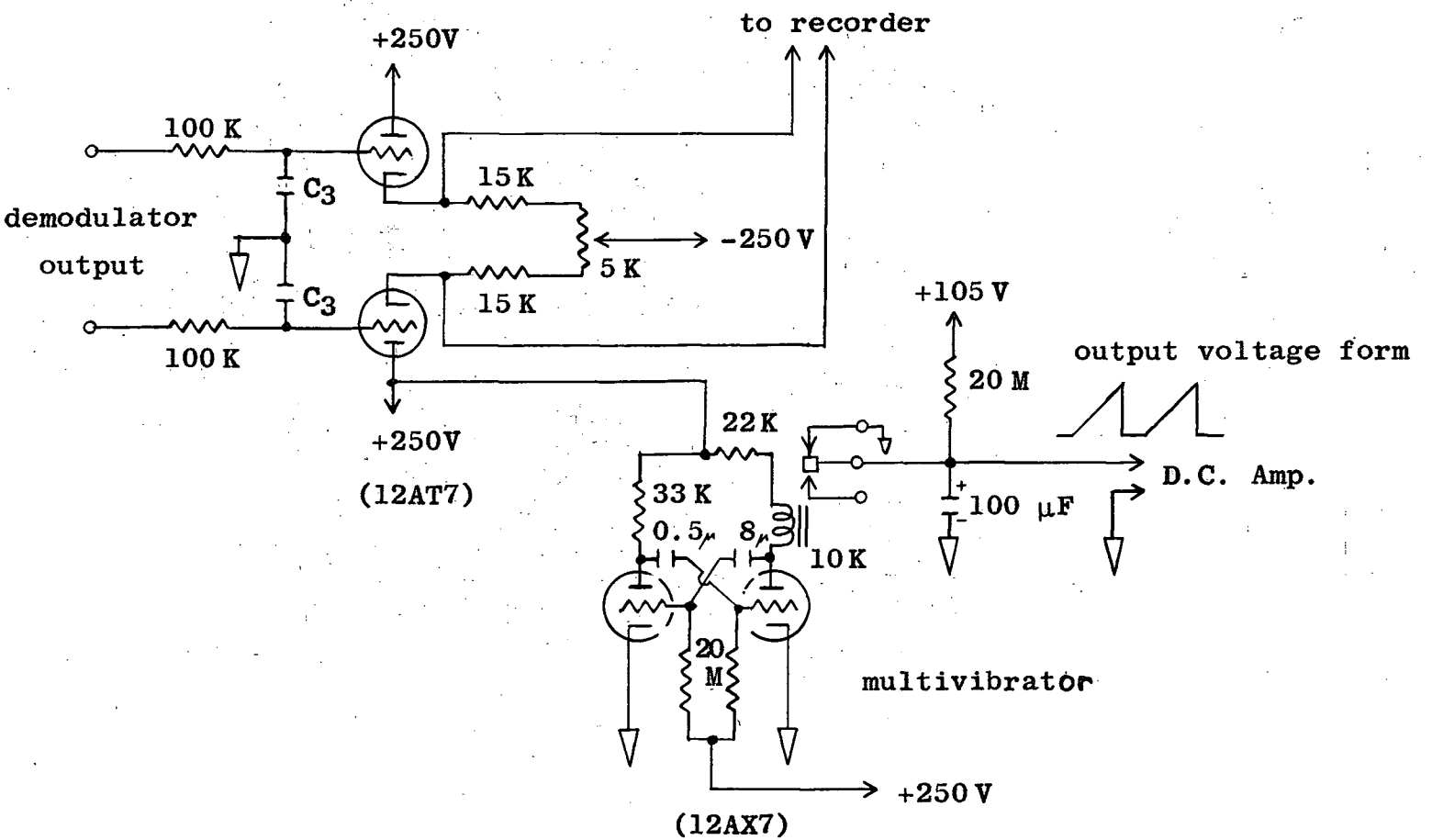

Fig. (30)

Search for u-mode Signal.

noise was greatly reduced. However, the eddy currents induced in the aluminum sheets caused a large leakage of the polarizing field into the receiving coil and it was necessary to inject a strong out of phase signal from the quartz crystal oscillator into the first stage of the A.C. amplifier in order to reduce the leakage amplitude. Otherwise, because of saturation of the third and fourth stages of the A.C. amplifier, as well as the demodulator, it was impossible to observe a signal.

An example of the nuclear magnetic resonance u-mode signal obtained is shown in Fig. (31). The half line width is approximately 500 γ compared to the optimum 1.87 γ predicted theoretically. The sensitivity at the recorder is read from the graph as 7.2 $\mu A/\gamma$. The current gain of the cathode follower is given by[21]

$$\frac{\Delta i_L}{\Delta e_g} \approx \frac{g_m}{2} \quad ,$$

where Δi_L = incremental plate current

Δe_g = incremental grid voltage

g_m = transconductance

and for the vacuum tube 12AT7,

$$g_m = 5.5 \text{ mA/V.}$$

Therefore, at the demodulator output the sensitivity is

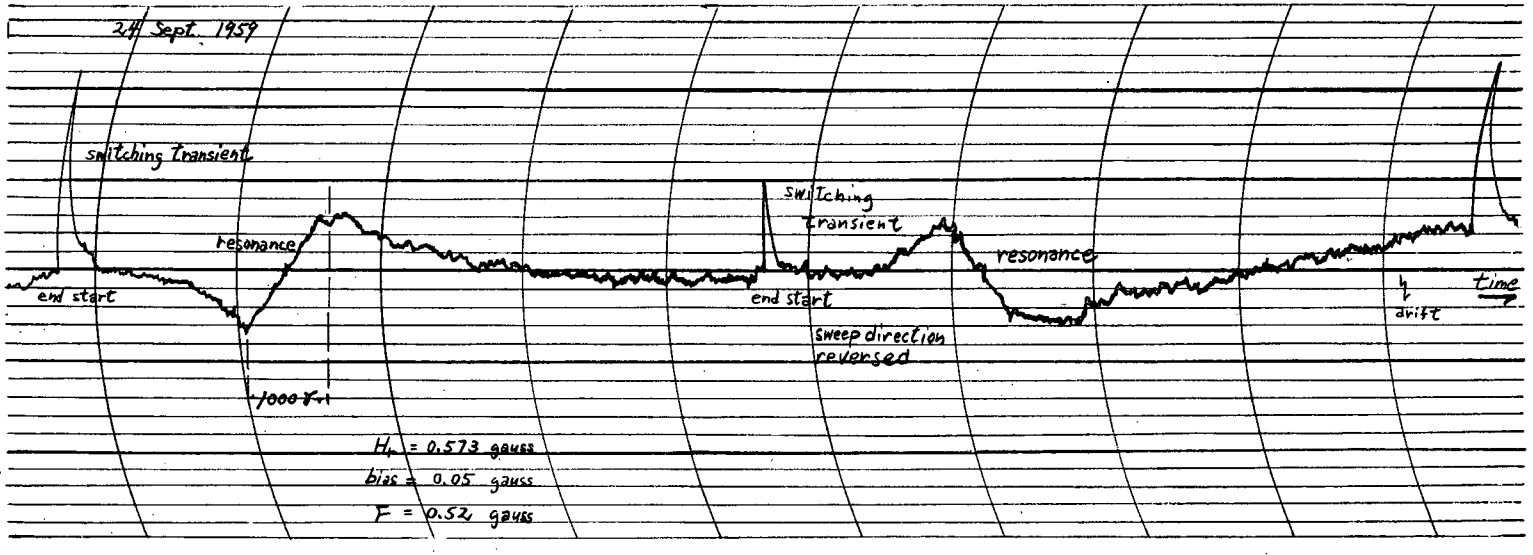

Note: The sweep in this case is a triangular wave form.

Fig. (31)

u-mode Signal.

1.3×10^{-3} V/γ. Multiplying this by the D.C. amplifier gain constant K_4 = 100 mA/V, we find the sensitivity of the open loop system K_f to be equal to 0.13 mA/γ, compared to 2.8 mA/γ predicted theoretically. However, for this open loop sensitivity the expected feedback system sensitivity is K $\approx$ 17 μA/γ compared to the theoretical prediction of 20 μA/γ, and the advantage of a feedback system is clearly indicated.

4.2 Effects of the Leakage of the Polarizing Magnetic Field $\overline{H}_p$.

The open loop sensitivity obtained in the previous section is very low compared to the theoretical value 2.8 mA/γ. The main cause of the low operational sensitivity is the strong leakage of the polarizing magnetic field into the receiving coil. In order to avoid saturation, the A.C. amplifier gain is kept low since the cancellation by injection of an out of phase signal is not perfect. Also the inhomogeneity of the magnetic field across the sample is relatively large for a sample of 5.8 liters and consequently T_2^* is short thereby reducing the slope of the u-mode signal.

The components comprising the amplitude control and phase shifting network of the injection circuit are extremely sensitive to electrical and mechanical shock and are also temperature dependent. Therefore, a rapid drift of the base line is present and frequent adjustments of

the injection controls are required. It was found impractical to attempt to close the feedback loop, much to the author's regret.

CHAPTER V

CONCLUSIONS AND SUGGESTIONS

It has been shown that it is possible to obtain a nuclear magnetic resonance signal at a low field value of 0.52 gauss. Since the feedback theory predicts a stable operation, the proposed feedback system will function as designed, provided that there is no drift in the base line of the demodulator output. A sensitivity of the order 20 $\mu A/\gamma$ can be expected. An increase in this figure can be realised by reducing the sensitivity of the feedback Helmholtz coil. The main cause of the drift of the base line is the variation of the phase and amplitude of the injection from the quartz crystal oscillator. There are two methods that can be applied without too much complication to reduce the drift to an acceptable level. The first is to choose an experimental site with a minimum of 60 c.p.s. noise. This may be impractical since the magnetometer is designed to operate from 60 c.p.s. A.C. mains, but conversion to operation from batteries is not difficult because of recent advances in transistorized D.C. to D.C. converters. Such a site would make operations without a Faraday shield possible and the leakage can be reduced to a minimum. The second method is to enclose the coil system into a large Faraday shield con-

sisting of wire mesh so that the polarizing field will not be affected by eddy currents.

An extremely simple system to avoid saturation is possible. Consider the block diagram shown in Fig. (32). The u-mode signal is demodulated after a single stage amplification. The D.C. signal obtained is then filtered to eliminate the nuclear magnetic resonance carrier frequency and fed into a modulator with a suitable carrier frequency. The modulated carrier signal is then amplified to a suitable level and demodulated. The system is free of saturation from the leakage. The section after the first demodulator can be a commercial high gain chopper amplifier which would greatly simplify the construction of a nuclear magnetic resonance magnetometer.

An interesting experiment to carry out would be the use of liquid hydrogen as the sample in the place of water. The population ratio of the two energy states of proton magnetic moments is a Boltzmann Distribution:

$$\frac{N(m_n = +\frac{1}{2})}{N(m_n = -\frac{1}{2})} = \left(\exp \frac{2mF}{kT}\right) \approx 1 + \frac{2mF}{kT} \quad .$$

Obviously the number of excess magnetic moments in the lower $m_n = +\frac{1}{2}$ energy states is given by

$$\frac{2mF}{kT} N(m_n = -\tfrac{1}{2}) \quad .$$

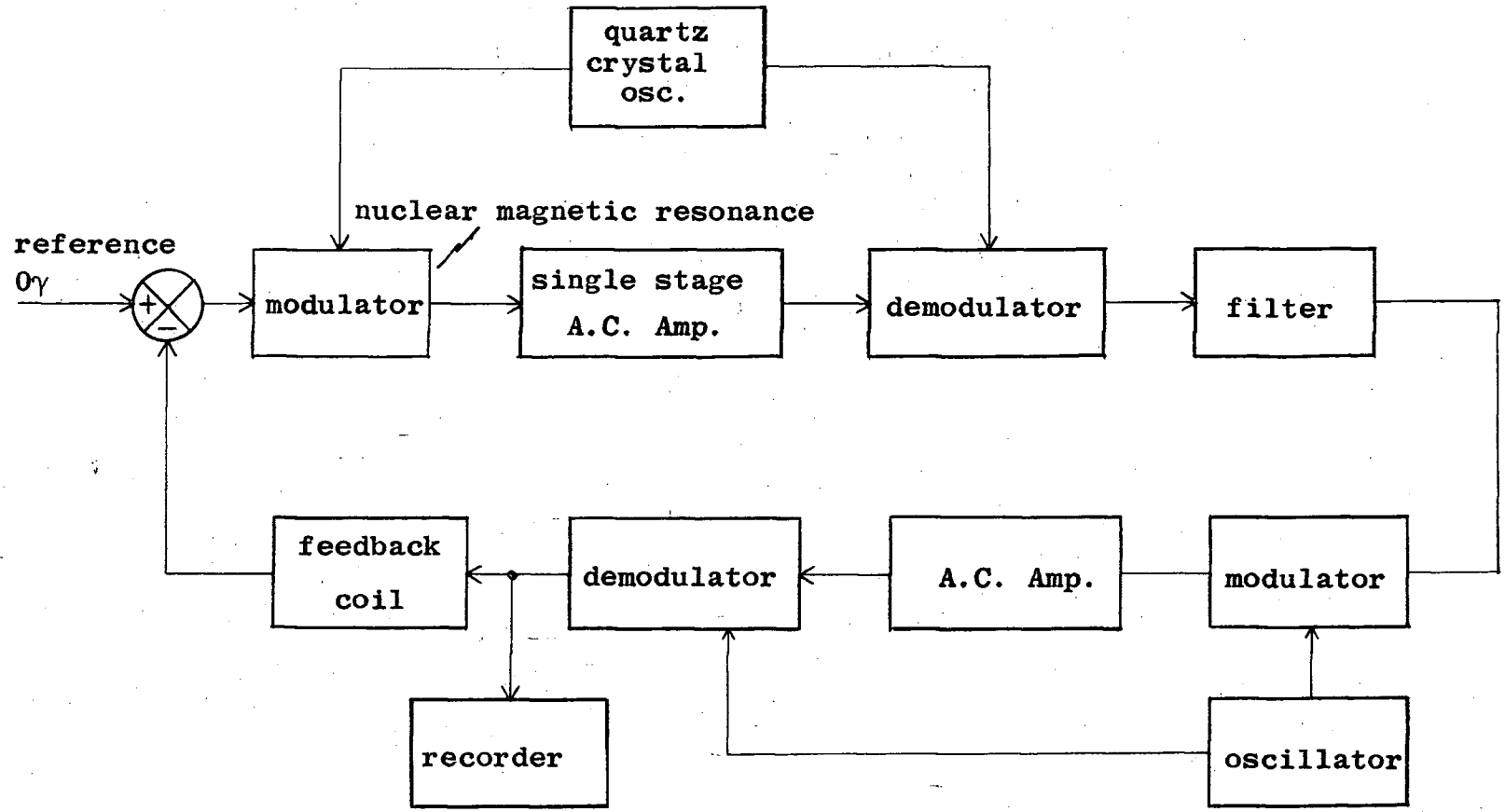

Fig. (32)

Nuclear Magnetic Resonance Magnetometer with no Saturation.

Therefore, at the temperature of liquid hydrogen, which is approximately 30°K, the macroscopic magnetic moment per unit volume is at least greater by a factor of 9. The density of free protons is lower by a factor of 0.67 compared to that of water. Thus an increase in sensitivity by a factor of 6 can be expected.

By applying some of the suggested improvements it should be possible to complete the magnetometer as a feedback system and obtain a constant frequency response beyond 10 c.p.s. with sensitivity down to 1 γ with a dynamic range in excess of 200 γ.

APPENDIX A

NUCLEAR MAGNETIC RESONANCE

A.1 A General Precession Theorem

A charged particle with angular momentum $\overline{a}$ has an associated magnetic moment $\overline{m}$ given by,

$$\overline{m} = \gamma \overline{a} \qquad \text{(A-1)}$$

where γ is a constant known as the gyromagnetic ratio. When the charged particle is placed in a magnetic field $\overline{F}$, a torque $\overline{T}$ acts on the magnetic moment $\overline{m}$, and the angular momentum changes at a rate equal to the torque; that is

$$\overline{T} = \frac{d\overline{a}}{dt} = \overline{m} \times \overline{F} = \gamma\, \overline{a} \times \overline{F} \; . \qquad \text{(A-2)}$$

To show that the magnetic moment $\overline{m}$ precesses about the magnetic field $\overline{F}$, equation (A-2) must be solved. Assuming that $\overline{F}$ is parallel to the z axis of a Cartesian coordinate system, equation (A-2) can be expressed as follows:

$$\begin{cases} \dfrac{da_x}{dt} = \gamma\, F\, a_y & \text{(A-3)} \\[2ex] \dfrac{da_y}{dt} = -\gamma\, F\, a_x & \text{(A-4)} \\[2ex] \dfrac{da_z}{dt} = 0 & \text{(A-5)} \end{cases}$$

Equation (A-5) shows that a_z, the component of the angular momentum $\bar{a}$ along the z axis, is constant. Therefore, the angle α between $\bar{a}$ and the magnetic field $\bar{F}$ is constant, and

$$a_z = a \cos \alpha \quad . \tag{A-6}$$

It follows from equations (A-3) and (A-4) that

$$\frac{d^2 a_x}{dt^2} + (\gamma F)^2 a_x = 0$$

This has a solution of the form

$$a_x = A \cos (-\gamma Ft + \theta) \tag{A-7}$$

where θ is a constant dependent on initial conditions. Similarly the component along the y axis of $\bar{a}$ is given by

$$a_y = A \sin (-\gamma Ft + \theta) \quad . \tag{A-8}$$

Since

$$a_x^2 + a_y^2 = A^2 = (a \sin \alpha)^2 \quad ,$$

equations (A-7) and (A-8) together with (A-6) give

$$\begin{cases} a_x = a \sin \alpha \cos (wt + \theta) \\ a_y = a \sin \alpha \sin (wt + \theta) \\ a_z = a \cos \alpha \end{cases} \tag{A-9}$$

where $\bar{w} = -\gamma \bar{F}$. Equation (A-9) is a solution of the vector

equation (A-2). The precession of the angular momentum $\bar{a}$ about the z axis is clearly shown, and from equation (A-1) it is seen that the magnetic moment $\bar{m}$ also precesses about the z axis. Figure (a-1) shows the relation between the various vectors.

A.2 Magnetic Resonance

If there are no relaxation forces present, the equation of motion for a particle with angular momentum $\bar{a}$ and magnetic moment $\bar{m}$ in a magnetic field $\bar{F}$ is given by equation (A-2).

$$\frac{d\bar{a}}{dt} = \gamma\, \bar{a} \times \bar{F} \qquad \text{(A-2)}$$

As was shown previously, $\bar{a}$ and $\bar{m}$ precess about $\bar{F}$ with angular velocity $\bar{w} = -\gamma\, \bar{F}$.

The effect of a rotating magnetic field on the precession is readily determined by transferring to a rotating coordinate system. The operator equation

$$\frac{d}{dt} = \frac{D}{Dt} + \bar{w}_r \times \qquad \text{(A-10)}$$

expresses the transformation of a first order derivative of a vector from a laboratory coordinate system to a rotating coordinate system. The symbol $\bar{w}_r$ represents the angular velocity of the rotating system, relative to the laboratory system. Applying equation (A-10) to (A-2), the following

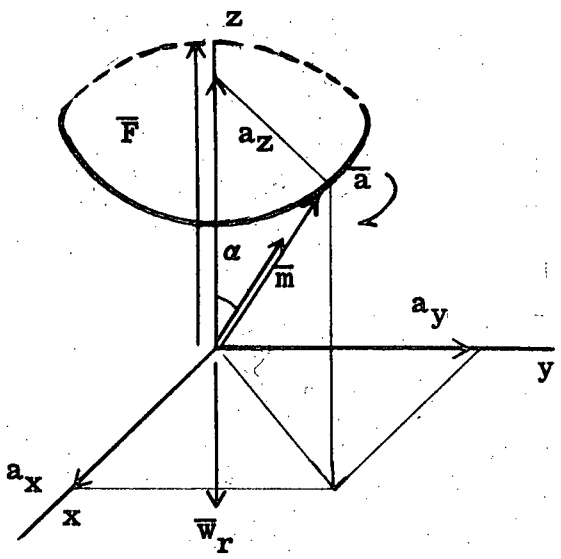

Fig. (a-1)

General Precession.

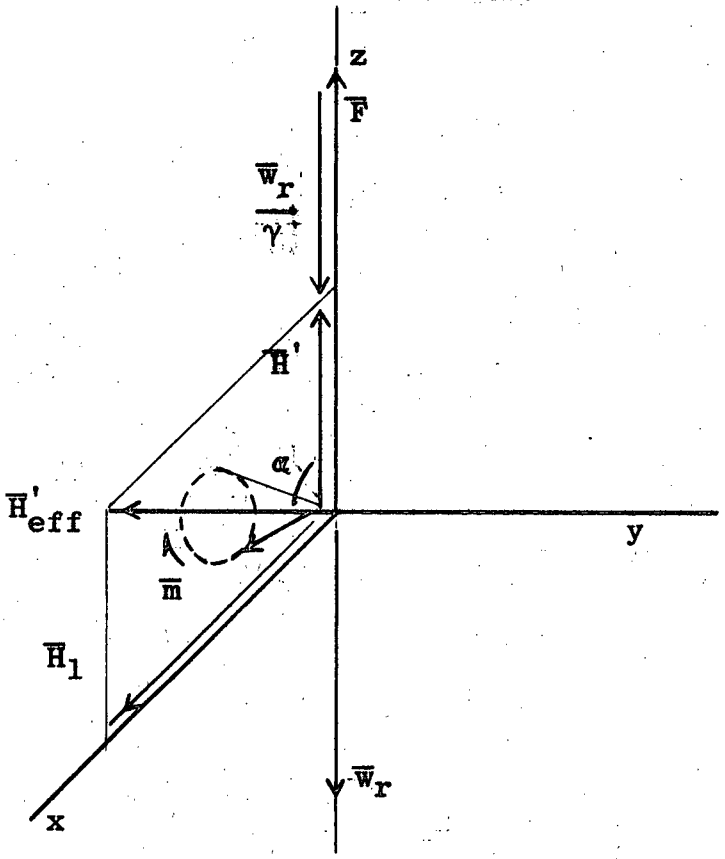

Fig. (a-2)

Magnetic Resonance.

expression is obtained:

$$\frac{D\bar{a}}{Dt} = \gamma\ \bar{a}\ x\ (\bar{F} + \frac{\bar{w}_r}{\gamma}) \qquad \text{(A-11)}$$

Equation (A-11) shows that in the rotating coordinate system the apparent magnetic field is

$$\bar{H}' = \bar{F} + \frac{\bar{w}_r}{\gamma}$$

and the apparent angular velocity of precession

$$\bar{w}' = -(\gamma\ \bar{F} + \bar{w}_r)\ .$$

If $\bar{w}_r = -\gamma\ \bar{F}$, then $\bar{H}'$ and $\bar{w}'$ are both zero, and the angular momentum $\bar{a}$ and magnetic moment $\bar{m}$ do not precess in the rotating coordinate system. For convenience, assume that a rotating magnetic field $\bar{H}'$ is applied in such a manner that it appears parallel to the x axis of the rotating coordinate system. The resultant magnetic field $\bar{H}'_{eff}$ in the rotating coordinate system is the vector sum of $\bar{H}_1$ and H', as shown in Fig. (a-2). The magnetic moment $\bar{m}$ now precesses about $\bar{H}'_{eff}$ with angular velocity $-\gamma\ \bar{H}'_{eff}$. When $\bar{w} = \bar{w}_r$, $\bar{H}'_{eff}$ becomes equal to $\bar{H}_1$ since $\bar{F} = -\frac{\bar{w}_r}{\gamma}$, and $\bar{m}$ will precess about the x axis of the rotating coordinate system. Therefore, the projection of $\bar{m}$ on to $\bar{F}$, the physically observable part m_F of the magnetic moment, will seem to vary between $+m_F$ and $-m_F$, where, in the case of protons, $-m_F$ is the

higher energy state and $+m_F$ the lower energy state. Obviously for an assembly of non-interacting protons the precession about $\overline{H}'_{eff}$ is a forced resonance phenomenon, known as magnetic resonance, whose observable amplitude is a maximum when the angular frequency $\overline{w}_r$ of the rotating magnetic field is equal to the Larmor precession frequency $\overline{w} = -\gamma \overline{F}$ of the protons.

When placed in a magnetic field $\overline{F}$, because of quantization, protons are allowed only two energy states which are determined by the magnetic quantum numbers $m_n = \pm\frac{1}{2}$. In actual experiments, where relaxation forces are present, the requirement of thermal equilibrium between the spin system and "lattice" prevents part of the proton magnetic moments from assuming the lower $m_n = +\frac{1}{2}$ state and the equilibrium condition established is a Boltzmann Distribution
The rotating magnetic field, in effect, induces transitions between the two energy states by forcing the magnetic moments to "flip" from one state to the other. Statistically, the transition probabilities from the $m_n = +\frac{1}{2}$ state to the $m_n = -\frac{1}{2}$ state and from the $m_n = -\frac{1}{2}$ state to the $m_n = +\frac{1}{2}$ state, are equal. Since, the lower $m = +\frac{1}{2}$ state has a higher population, the number of transitions from the lower state to the higher state exceeds the transitions from the higher state to the lower state. The higher $m_n = -\frac{1}{2}$ state population increases until an equilibrium is achieved between the energy dissipation to the lattice from the

proton assembly, and the energy input to the assembly from the rotating magnetic field. To maintain the equilibrium condition the rotating magnetic field must be applied continuously. As a result of the magnetic resonance effect the macroscopic magnetic moment $\overline{M}$ of the proton assembly is reduced in magnitude. This is due to the smaller population difference of the two energy states.

A.3 The Bloch Equations

Consider a paramagnetic substance subjected to a magnetic field $\overline{F}$ which is applied parallel to the z axis of a Cartesian coordinate system. According to the Curie-Langevin Theory[21] the macroscopic magnetic moment $\overline{M}$ must ultimately attain an equilibrium value $M_o = XF$ (X = nuclear paramagnetic susceptibility) along the direction of the magnetic field $\overline{F}$, and the x and y components of $\overline{M}$ will vanish. Therefore, nuclear magnetic moments such as the protons in hydrogen cannot be considered as an assembly of non-interacting magnetic moments free from external effects and several factors affecting their equilibrium condition must be taken into account. There are three main factors to be considered:

(1) Atomic or molecular magnetism

(2) Spin-lattice interaction

and (3) Spin-spin interaction.

The factor (1) is generally avoided by the use of

diamagnetic substances such as water.

The factor (2) accounts for the thermal motions of the nuclear spin system. Dissipation of energy takes place through the interaction of the spin system with the "lattice". If M_z is the instantaneous z component of $\overline{M}$ in the steady magnetic field $\overline{F}$, then the energy of the nuclear spin system is

$$W = -M_z F \ .$$

But according to the Curie-Langevin Theory the equilibrium energy is

$$W = -M_o F \ .$$

Therefore, M_z will tend to the equilibrium value M_o at a rate determined by the degree of thermal motion. If a simple exponential law is assumed, the dynamic condition can be expressed by

$$\frac{dM_z}{dt} = \frac{1}{T_1} (M_o - M_z) \qquad \text{(A-12)}$$

where T_1 is the spin-lattice relaxation time or the longitudinal relaxation time. It is a measure of the time required for $\overline{M}$ to attain thermal equilibrium with the lattice, when the z component of $\overline{M}$ becomes equal to the equilibrium value M_o. The solution of equation (A-12) is of the form

$$M_z = M_o \left\{ 1-\exp(-\frac{t}{T_1}) \right\}$$

where the initial value of M_z is taken to be zero.

The third factor (3) accounts for the interaction among the nuclear magnetic moments of the spin system. It is mainly the components M_x and M_y of the macroscopic magnetization $\overline{M}$ that are affected because of the tendency of the spin-spin interaction to make the nuclear magnetic moments precess with incoherent phase about the magnetic field $\overline{F}$, which is parallel to the z axis. The approach to the equilibrium value, zero, by M_x and M_y can be expressed as,

$$\begin{cases} \dfrac{dM_x}{dt} + \dfrac{M_x}{T_2} = 0 \\ \\ \dfrac{dM_y}{dt} + \dfrac{M_y}{T_2} = 0 \end{cases} \qquad \text{(A-13)}$$

where T_2 is the spin-spin relaxation time or the transverse relaxation time. It is a measure of the time required for a group of precessing magnetic moments, initially in phase with each other, to become out of phase. The inhomogeneity of $\overline{F}$ across the sample will also contribute to the phase incoherence of the precessing magnetic moments. When this effect is also taken into account, T_2 is written as T_2^*. Solutions of equation (A-13) are of the form

$$M_x = M_x(0) \exp\left(-\frac{t}{T_2}\right)$$

and

$$M_y = M_y(0) \exp\left(-\frac{t}{T_2}\right) .$$

The equation expressing the dynamical condition of a particle with angular momentum $\bar{a}$ and magnetic moment $\bar{m}$ subjected to a magnetic field $\bar{F}$ is given by

$$\frac{d\bar{a}}{dt} = \bar{m} \times \bar{F} \qquad \text{(A-2)}$$

Since $\bar{m} = \gamma \bar{a}$, equation (A-2) becomes

$$\frac{d\bar{m}}{dt} = \gamma \bar{m} \times \bar{F} \qquad \text{(A-14)}$$

By analogy, the dynamical condition of the macroscopic magnetic moment $\bar{M}$ can be expressed as

$$\frac{d\bar{M}}{dt} = \gamma \bar{M} \times \bar{F} \qquad \text{(A-15)}$$

where relaxation effects are assumed to be absent. To include the effects of relaxation forces, equation (A-15) is combined with equations (A-12) and (A-13) to obtain the expression

$$\frac{d\bar{M}}{dt} + \bar{i}\,\frac{M_x}{T_2^*} + \bar{j}\,\frac{M_y}{T_2^*} + \bar{k}\,\frac{(M_z - M_o)}{T_1} = \gamma \bar{M} \times \bar{F} \qquad \text{(A-16)}$$

If a rotating magnetic field, given by

$$\begin{cases} H_x = H_1 \cos w_r t \\ H_y = -H_1 \sin w_r t \end{cases} \qquad \text{(A-17)}$$

is superimposed on the magnetic field $\bar{F}$, which is parallel

to the z axis, equation (A-16) becomes

$$\frac{d\bar{M}}{dt} + \bar{i}\frac{M_x}{T_2^*} + \bar{j}\frac{M_y}{T_2^*} + \bar{k}\frac{(M_z - M_o)}{T_1}$$

$$= \gamma \bar{M} \times (\bar{i} H_1 \cos w_r t - \bar{j} H_1 \sin w_r t + \bar{k} F) \qquad \text{(A-18)}$$

In terms of its components, equation (A-18) can be written,

$$\frac{dM_x}{dt} + \frac{M_x}{T_2^*} = \gamma M_y F + \gamma M_z H_1 \sin w_r t \qquad \text{(A-19)}$$

$$\frac{dM_y}{dt} + \frac{M_y}{T_2^*} = -\gamma M_x F + \gamma M_z H_1 \cos w_r t \qquad \text{(A-20)}$$

$$\frac{dM_z}{dt} + \frac{M_z - M_o}{T_1} = -\gamma M_x H_1 \sin w_r t + \gamma M_y H_1 \cos w_r t \qquad \text{(A-21)}$$

Equations (A-19), (A-20) and (A-21) are known as the Bloch Equations.

The Bloch equations can be simplified by transforming from the laboratory Cartesian coordinate system to a rotating Cartesian coordinate system which has angular velocity $-\bar{w}_r$, relative to the laboratory system, and z axis coincident with the laboratory system. Referring to Fig. (a-3), the components u and v of the macroscopic magnetic moment $\bar{M}$, in the rotating system are given by

$$u = M_x \cos w_r t - M_y \sin w_r t \qquad \text{(A-22)}$$

and

$$v = -(M_x \sin w_r t + M_y \cos w_r t) \qquad \text{(A-23)}.$$

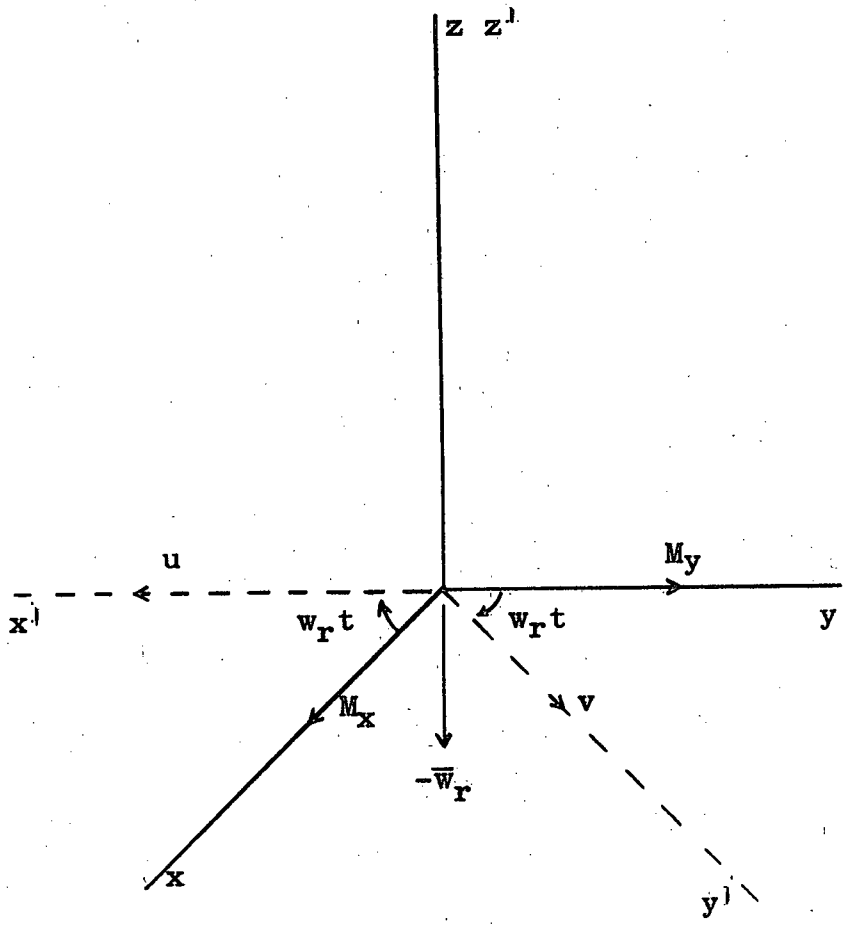

Fig. (a-3)

Components of M_x and M_y in Rotating Coordinates.

It is readily shown that

$$M_x = u \cos w_r t - v \sin w_r t \qquad \text{(A-24)}$$

and

$$M_y = -(u \sin w_r t + v \cos w_r t) \qquad \text{(A-25)}$$

Applying equation (A-24) and (A-25) to the Bloch equations (A-19), (A-20) and (A-21), the following expressions are obtained:

$$\frac{du}{dt} = -(\gamma F - w_r) v - \frac{u}{T_2^*} \qquad \text{(A-26)}$$

$$\frac{dv}{dt} = (\gamma F - w_r) u - \frac{v}{T_2^*} - \gamma H_1 M_z \qquad \text{(A-27)}$$

and

$$\frac{dM_z}{dt} = \frac{M_o - M_z}{T_1} + \gamma H_1 v \qquad \text{(A-28).}$$

For simplicity let the magnetic field $\overline{F}$ be constant. Then the nuclear spin system can be considered to be in thermal equilibrium, and

$$\frac{du}{dt} = \frac{dv}{dt} = \frac{dM_z}{dt} = 0 \quad .$$

It follows that, putting $w_r = \gamma H_r$,

$$u = -T_2^* \gamma (F - H_r) v \qquad \text{(A-29)}$$

$$v = - \frac{H_1 M_z \gamma T_2^*}{1 + (\gamma T_2^*)^2 (F - H_r)^2} \qquad \text{(A-30)}$$

and

$$M_z = M_o \frac{1 + (\gamma T_2^*)^2 (F - H_r)^2}{1 + (\gamma H_1)^2 T_1 T_2^* + (\gamma T_2^*)^2 (F - H_r)^2} \qquad \text{(A-31)}$$

Substituting equation (A-31) into (A-30) the solution for v is obtained:

$$v = \frac{H_1 M_o \gamma T_2^*}{1 + (\gamma H_1)^2 T_1 T_2^* + (\gamma T_2^*)^2 (F - H_r)^2} \qquad \text{(A-32)}$$

Substituting equation (A-32) into (A-29) in turn gives the solution for u:

$$u = \frac{H_1 M_o (\gamma T_2^*)^2 (F - H_r)}{1 + (\gamma H_1)^2 T_1 T_2^* + (\gamma T_2^*)^2 (F - H_r)^2} \qquad \text{(A-33)}$$

Since the expression for M_y is given by equation (A-25) as

$$M_y = -(u \sin w_r t + v \cos w_r t) ,$$

the signal detected by crossed coil nuclear magnetic resonance experiments is now known.

The general shapes of u and v as a function of $\triangle F = F - H_r$ are shown in Fig. (a-4). Differentiating equation (A-33) with respect to $\triangle F$ gives

$$\frac{du}{d(\triangle F)} = \frac{H_1 M_o (\gamma T_2^*)^2 \left\{ 1 + (\gamma H_1)^2 T_1 T_2^* - (\gamma T_2^*)^2 (F - H_r)^2 \right\}}{\left\{ 1 + (\gamma H_1)^2 T_1 T_2^* + (\gamma T_2^*)^2 (F - H_r)^2 \right\}^2} \qquad \text{(A-34)}$$

Therefore the maxima and minima of u are given by

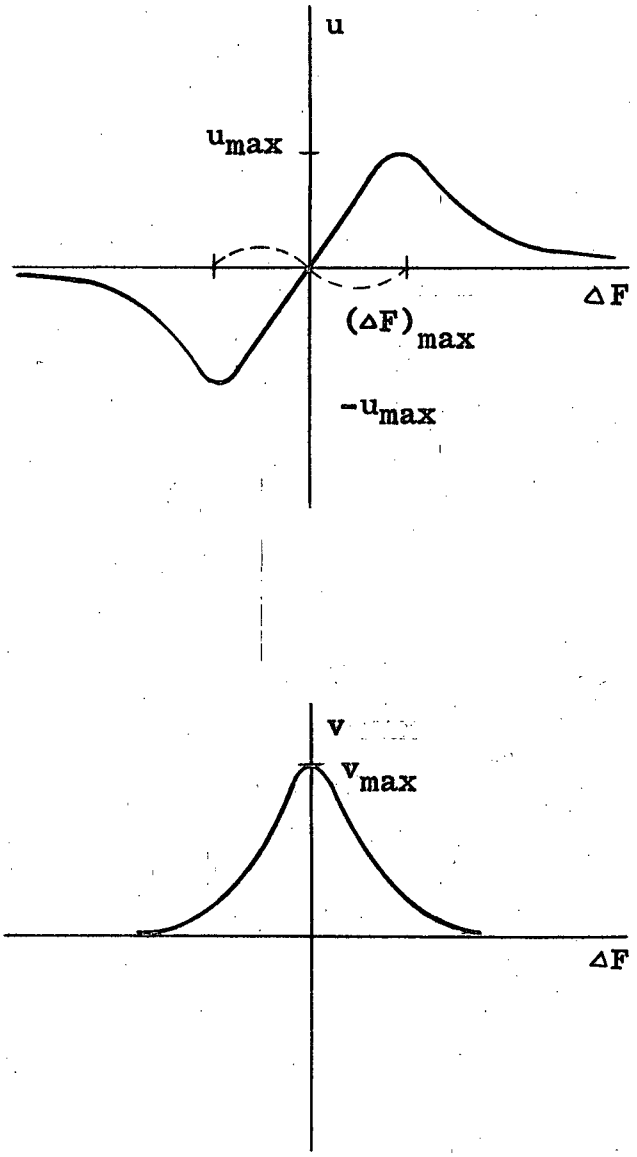

Fig. (a-4)

The Graphical Form of u and v.

$$u_{max} = \pm \frac{1}{2} \cdot \frac{\gamma H_1 T_2^* M_o}{\left\{1 + (\gamma H_1)^2 T_1 T_2^*\right\}^{\frac{1}{2}}}$$

when

$$\Delta F = (\Delta F)_{max} = \pm \frac{1}{\gamma T_2^*} \left\{1 + (\gamma H_1) \; T_1 T_2^*\right\}^{\frac{1}{2}} .$$

The magnitude of u_{max} increases monotonically with H_1 but tends to an asymptotic value

$$(u_{max})_{max} = \frac{M_o}{2} \left(\frac{T_2^*}{T_1}\right)^{\frac{1}{2}} .$$

The magnitude of v reaches the maximum value

$$v_{max} = \frac{H_1 M_o \gamma T_2^*}{1 + (\gamma H_1)^2 T_1 T_2^*}$$

at $\Delta F = 0$. The magnitude of v_{max} increases at first as H_1 increases and reaches a maximum value

$$(v_{max})_{max} = \frac{M_o}{2} \left(\frac{T_2^*}{T_1}\right)^{\frac{1}{2}}$$

when

$$(\gamma H_1)^2 T_1 T_2^* = 1 .$$

Thus the maximum values that u_{max} and v_{max} can attain are equal.

Bloch has shown that the solution of the Bloch equations obtained, thus far, also hold for slow variations of $\overline{F}$ [22][23], provided

$$\left| \frac{d}{dt} \left(\frac{F - H_r}{H_1} \right) \right| \ll \gamma H_1 \quad .$$

Under this condition it can be regarded that the steady state of thermal equilibrium is attained at each instant. Therefore the solution will continue to be valid with $\overline{F}$ now representing the instantaneous value of the magnetic field applied.

In the application of nuclear magnetic resonance to the magnetometer, the u-mode signal is utilized. Since the variation of the geomagnetic field magnitude is generally kept to less than 0.1% of the main field by the feedback system, it is found convenient to assume that the thermal equilibrium value of the macroscopic magnetization M_o is equal to

$$M_o = M = X H_r$$

where X is the nuclear paramagnetic susceptibility and H_r the resonance value of F. For protons in water at room temperature X is given by the Curie formula [24]

$$X = n \frac{(I + 1)}{3 I} \frac{m^2}{kT} = 3.4 \times 10^{-10}$$

where $n = 6.9 \times 10^{22}/cm^3$, the number of hydrogen atoms per unit volume in water.

$I = \frac{1}{2}$, the nuclear spin number.

$m = 1.4 \times 10^{-23}$ c.g.s., the magnetic moment of a proton.

k = Boltzmann's constant

and T = 291° K.

APPENDIX B

FEEDBACK SYSTEM ANALYSIS*

B.1 Classification of Systems

Definitions:

Linear System:

A system whose state can be expressed by a linear differential equation of the form

$$a_n \frac{d^n x}{dt^n} + a_{n-1} \frac{d^{n-1} x}{dt^{n-1}} + \ldots + a_o x(t)$$

$$= b_m \frac{d^m f}{dt^m} + b_{m-1} \frac{d^{m-1} f}{dt^m} + \ldots + b_o f(t)$$

where $x(t)$ is the response, output or dependent variable and $f(t)$ is the input or driving function. The symbol t is the independent variable and usually denotes time. In most physical systems a_i, $(i = 0,1,2,\ldots n)$ and b_r, $(r = 0,1,2,\ldots m)$ are constants.

Feedback System:

A system where some function of the output, or the output of part of the system, is reintroduced as a secondary driving function so as to modify the output. A block diagram of such a system is shown in Fig. (b-1).

---

* A list of references is given at the end of the thesis.

Servo System:

A feedback system where the output is compared with the input, which is the desired output, and the driving element or amplifier is activated by the difference between the two quantities. A block diagram of such a system is shown in Fig. (b-2).

It is readily seen that a servo system is a special case of a feedback system. The term "servomechanism" usually refers to servo systems involving mechanical elements where such elements introduce the dominating time constant of the system.

A simple remote control system with zero feedback is sometimes known as a "slave servo", or more appropriately, an "open loop system". Consequently a system with feedback is termed a "closed loop system". It should be noted that depending on the viewpoint taken, all the terms given above may be applied to the same system.

B.2 Laplace Transforms

A convenient method of solving linear differential equations with constant coefficients is the Laplace transform method. The method also lends itself readily to the analysis of feedback systems.

The Laplace transform of g(t) is defined as

$$G(s) = L\left\{ g(t) \right\} = \lim_{\lambda \to 0} \int_{\lambda}^{+\infty} g(t) \exp(-st)\, dt$$

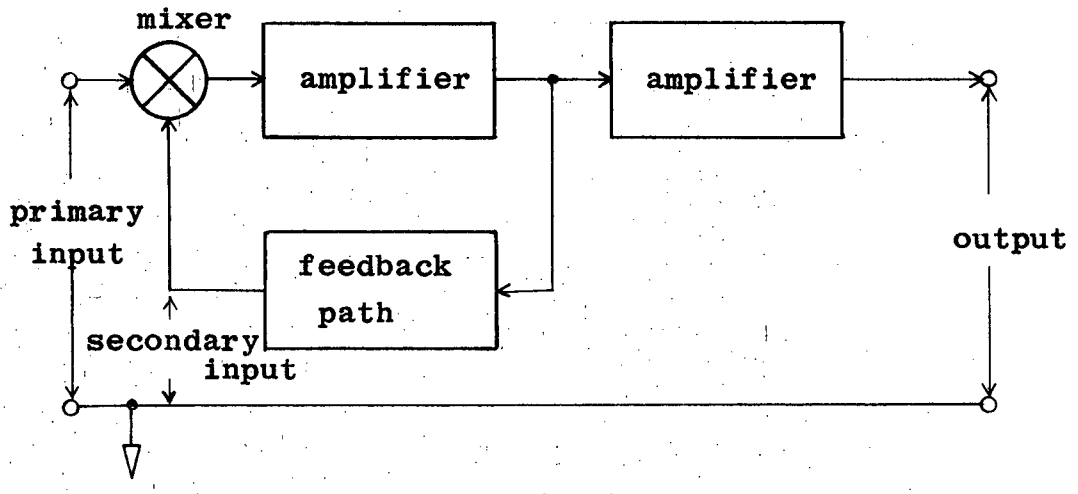

Fig. (b-1)

Feedback System.

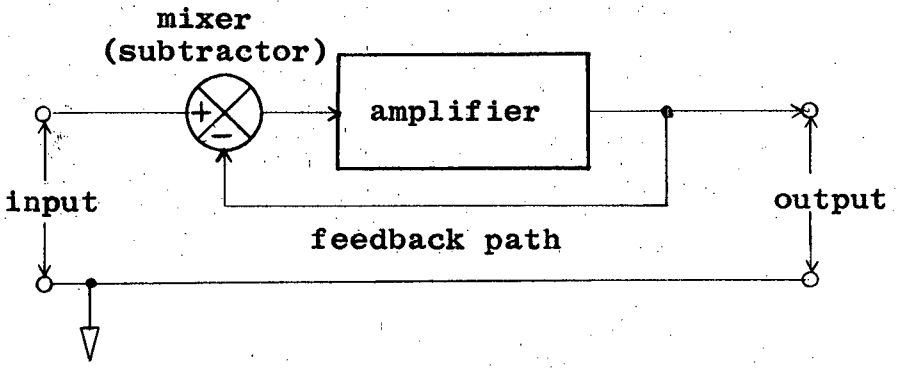

Fig. (b-2)

Servo System.

where $\lambda > 0$, $g(t) = A \exp(\alpha t)$ and $g(t) \equiv 0$ for $t < 0$. The symbols A and α are positive constants. For simplicity the transform is usually written without the limit sign as follows:

$$G(s) = L\left\{g(t)\right\} = \int_0^\infty g(t)\, e^{-st}\, dt \,.$$

Of immediate interest is the application of the transform to the solution of linear differential equations. Consider the differential equation

$$a_n \frac{d^n x}{dt^n} + a_{n-1} \frac{d^{n-1} x}{dt^{n-1}} + \ldots + a_o\, x(t)$$

$$= b_m \frac{d^m f}{dt^m} + \ldots + b_o\, f(t) \qquad \text{(B-1)}\,.$$

Since

$$L\left\{\frac{d^n f}{dt^n}\right\} = s^n F(s) - s^{n-1} F(0) - \ldots - F^{(n)}(0),$$

if zero initial conditions are assumed, which will be the case in most electrical systems, equation (B-1) yields,

$$(a_n s^n + a_{n-1}\, s^{n-1} + \ldots + a_o)\; L\left\{x(t)\right\}$$

$$= (b_m s^m + \ldots + b_o)\; L\left\{f(t)\right\} \,.$$

Putting

$$Y(s) = \frac{b_m s^m + \ldots + b_o}{a_n s^n + \ldots + a_o} \qquad \text{(B-2)}$$

we obtain

$$L\left\{x(t)\right\} = Y(s)\, L\left\{f(t)\right\} \quad . \tag{B-3}$$

The output, or response x(t) is found by finding the inverse Laplace transform of the right hand side of equation (B-3).

B.3 Inverse Laplace Transforms

The inverse Laplace transform of G(s) is defined as

$$g(t) = L^{-1}\left\{G(s)\right\} = \frac{1}{2\pi j}\int_{\alpha_1 - j\infty}^{\alpha_1 + j\infty} G(s)\exp(st)\, ds$$

where $\alpha_1 > \alpha$ and the path of integration is the Bromwich Contour which extends from $\alpha_1 - j\infty$ to $\alpha_1 + j\infty$ in the complex plane.

Thus, s is a complex number. In most cases it is possible to resolve the Laplace transform of G(s) into parts with recognizable inverses. When G(s) has a complicated form, methods of complex variable theory must be applied.

B.4 Transfer Function

The transfer function (system function, immitance function or transmission ratio) of a system is defined as follows:

The transfer function of a system is the ratio

of the system output to the system input provided that the system input, output and all currents and voltages are initially equal to zero.

The term transfer function is not normally associated with expressions of the input and output function in the time domain since their ratio does not occur naturally in the integro-differential equation describing a physical system. Equation (B-2) gives the transfer function of a system since from (B-3)

$$Y(s) = \frac{L\{x(t)\}}{L\{f(t)\}} = \frac{X(s)}{F(s)} \quad .$$

The closed loop or system transfer function of a feedback system is obtained by considering the block diagram of a generalized feedback system shown in Fig. (b-3). The symbol G(s) is the forward (open loop) transfer function and H(s) is the feedback transfer function. The loop transfer function is the product G(s) H(s) of the two transfer functions. Referring to Fig. (b-3), from the definition of a transfer function we have,

$$G(s) = \frac{V_o(s)}{E(s)} \text{ and } H(s) = \frac{V_f(s)}{V_o(s)} \quad .$$

Hence,

$$V_o(s) = E(s)G(s) \text{ and } V_f(s) = V_o(s)H(s) \ ,$$

and also

$$E(s) = V_i(s) - V_o(s)\ H(s) \ .$$

Therefore, the feedback system transfer function is given by

$$Y(s) = \frac{V_o(s)}{V_i(s)} = \frac{E(s)\ G(s)}{E(s) + V_o(s)\ H(s)} \ .$$

Dividing by E(s) we obtain

$$Y(s) = \frac{G(s)}{1 + H(s)\ G(s)} \ .$$

Note that the mixer is defined as a subtracting device, thereby producing the negative feedback effect. If the mixer is defined as an adding device, the feedback will be positive.

When H(s) = 1, the system transfer function becomes

$$Y(s) = \frac{G(s)}{1 + G(s)} \ .$$

A system with such a transfer function, where one hundred percent feedback is performed, is known as a servo system. It is a special case of a feedback system.

B.5 Transient Analysis

The response of a system to impulse inputs is

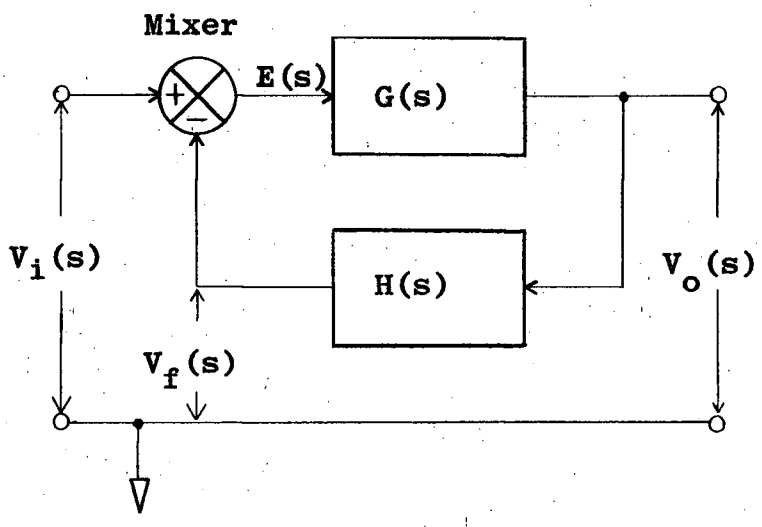

$V_i(s)$ = input to the feedback system

$V_f(s)$ = feedback

$E(s)$ = error input to the forward amplifier

$V_o(s)$ = output of the feedback system

Fig. (b-3)

Feedback System.

revealed by the inverse Laplace transform of the system transfer function, since for a unit impulse $\delta(t)$ the response is

$$x(t) = L^{-1}\left\{ 1 \cdot Y(s)\right\} = L^{-1}\left\{ Y(s)\right\} ,$$

where

$$\int_{-t_1}^{t_2} \delta(t)\, d\, t = 1, \quad t_1 \text{ and } t_2 > 0 ,$$

and

$$L\left\{ \delta(t)\right\} = 1 .$$

Therefore, the stability of a system is known when the inverse Laplace transform of the system transfer function is determined. The usual form of a transfer function is a rational function which can be expressed as

$$Y(s) = K \frac{(S - \lambda_1)(S - \lambda_2)\ldots(S - \lambda_n)}{(S - \alpha_1)(S - \alpha_2)\ldots(S - \alpha_m)}$$

where $m > n$. The symbols λ_1, λ_2 ... λ_n and α_1, α_2 ... α_n are constants termed as the zeros and poles of Y(s) respectively. From complex variable theory we have

$$L^{-1}\left\{ Y(s)\right\} = \frac{1}{2\pi j} \oint \frac{(S - \lambda_1)\ldots(S - \lambda_n)}{(S - \alpha_1)\ldots(S - \alpha_m)} \exp(st)ds$$

Cauchy's residue theorem is useful in obtaining the in-

verse and states that

$$\frac{1}{2\pi j}\oint \frac{F(s)}{(s-\alpha)^n}\,ds = F^{(n-1)}(s)\Big]_{s=\alpha}$$

It is readily shown that the position of the poles α_1, α_2 ... α_m in the complex plane determines the stability of the system since the exponent of the exponential function is given by the poles. In other words, poles with negative real parts will give a response that will decay as t increases but poles with positive real parts will give a response that increases with t and cause an unstable response. The method known as the Root-Locus method is used to determine the degree of stability of a system and its dependence on the system parameters.

B.6 Steady State Analysis

The method of analysis by the steady state response of a system to a sinusoidal input has two advantages over the transient response analysis:

(1) The application of the method is simple for transfer functions with many zeros and poles.

(2) Design steps to improve the system are readily applied.

When the complex variable s in the system transfer function G(s) is replaced by s = jw, where w is the angular frequency, the transfer function is called the

frequency transfer function. It is identified as the transfer function representing the steady state relation between a continuous sinusoidal input and output, and leads to the representation of the response of a system as a Fourier Spectrum. It is readily shown that for an input of the form

$$v_i(t) = \sum_{n=1}^{k} a_n e^{-jw_n t}$$

the steady state output of a linear system is

$$v_o(t) = \sum_{n=1}^{k} a_n \, G(jw_n) \, e^{jw_n t} \, , \qquad \text{(B-4)}$$

where G(s) is the system transfer function. In order to find the steady state response it is necessary to know the nature of G(jw), the frequency transfer function.

From equation (B-4) it is seen that if G(jw) is plotted against frequency w, a representation of the gain of the system to sinusoidal inputs with unity amplitude will be obtained. Consider a loop transfer function of a negative feedback system which has the form

$$G(jw) = K(jw)^r \frac{(jwT_1+1)(jwT_3+1)\ldots(jwT_{2n+1}+1)}{(jwT_2+1)(jwT_4+1)\ldots(jwT_{2m+1}+1)} \qquad \text{(B-5)}$$

where r and K are constants and each T_i (i = 1,2,3,...) is a real constant known as the time constant associated with a group of elements in the system which produce the

particular pole or zero. Rewriting equation (B-5) in polar form using

$$\alpha + j\lambda = (\alpha^2 + \lambda^2)^{\frac{1}{2}} \exp(j\phi)$$

we obtain

$$G(jw) = K\left\{w\exp(j\tfrac{\pi}{2})\right\}^r \frac{\left\{(wT_1)^2+1\right\}^{\frac{1}{2}}\exp(j\phi_1)\left\{(wT_3)^2+1\right\}^{\frac{1}{2}}\exp(j\phi_3)\ldots}{\left\{(wT_2)^2+1\right\}^{\frac{1}{2}}\exp(j\phi_2)\left\{(wT_4)^2+1\right\}^{\frac{1}{2}}\exp(j\phi_4)\ldots}$$

where $\phi_i = \arctan wT_i$.

Taking the natural logarithm of both sides

$$\begin{aligned}\ln G(jw) = {} & \ln K + r\ln w + \ln\left\{(wT_1)^2+1\right\}^{\frac{1}{2}} + \ldots + \ln\left\{(wT_{2n+1})^2+1\right\}^{\frac{1}{2}} \\ & - \ln\left\{(wT_1)^2+1\right\}^{\frac{1}{2}} - \ldots - \ln\left\{(wT_{2m})^2+1\right\}^{\frac{1}{2}} \\ & + jr\tfrac{\pi}{2} + j\arctan wT_1 + \ldots + j\arctan wT_{2n+1} \\ & - j\arctan wT_2 - \ldots - j\arctan wT_{2m} \ .\end{aligned}$$

Essentially we have

$$\ln G(jw) = \ln A(w) + j\phi(w) \qquad \text{(B-6)}$$

where A(w) is the amplitude of G(jw) and $\phi(w)$ is the phase angle. Since G(jw) is the loop transfer function, equation (B-6) shows that if the phase angle, which represents the phase shift of a sinusoidal input after it has passed through the system, is larger than $\pm\pi$ at some frequency, the intended negative feedback will become a positive feed-

back and the system will oscillate. However, if the amplitude A(w) of the system is less than unity at the frequency of $\pm\pi$ phase shift, oscillations will not take place. Therefore, a graphical representation of the amplitude A(w) of G(jw) and the phase angle $\phi(w)$ with respect to frequency will reveal the stability of a system. To represent graphically the amplitude and phase angle of G(jw) against frequency w it is convenient to convert the natural logarithm to the decibel (db) magnitude which is defined as

$$\text{db amplitude} = 20 \log \frac{A_2}{A_1}$$

where A_1 and A_2 are the input and output amplitudes of sinusoidal functions. Since

$$\ln x = 2.30 \log x$$

we have

$$\text{db } |G(jw)| = 20 \log A(w) = \frac{20}{2.30} \ln A(w) \ .$$

The diagrams produced by plotting the decibel amplitude, db $|G(jw)|$, of the loop transfer function and phase angle $\phi(w)$ against logarithmic frequency log w, are known as Bode Diagrams. The asymptotic approximations which are readily derived, simplify the plotting of Bode Diagrams. Consider the n^{th} order zero and pole at the origin. We

have

$$\ln(jw)^{\pm n} = \pm n \ln w \pm jn \frac{\pi}{2}$$

Hence,

$$\text{db amplitude} = 20 \log \left| (jw)^{\pm n} \right| = \pm 20\, n \log w$$

and the phase angle is $\pm n \frac{\pi}{2}$. The slope of the decibel amplitude plotted against logarithmic frequency is approximately 6n db/octave since

$$\triangle \text{db} = 20n \log 2w - 20n \log w = 20n \log 2 \approx 6n \ .$$

The Bode Diagram of a first order pole and zero at the origin is shown in Fig. (b-4), together with the plot of the constant gain factor K.

The Bode Diagram of an n^{th} order real zero and pole are derived in a similar manner. We have

$$\ln(jwT+1)^{\pm n} = \pm n \ln \left\{ (jwT)^2 + 1 \right\}^{\frac{1}{2}} \pm jn \arctan wT$$

Therefore,

$$\text{db amplitude} = 20 \log \left| (jwT + 1)^{\pm n} \right| = \pm 20n \log \left\{ (jwT)^2 + 1 \right\}^{\frac{1}{2}}$$

and the phase angle is $\pm n \arctan wT$. Asymptotic approximations are;

for $wT \ll 1$ db amplitude $\approx \pm 20n \log 1 = 0$

and for $wT \gg 1$ db amplitude $\approx \pm 20n \log wT$

which has a slope $\pm 6n$ db/oct.

Also when $w = 1/T$,

$$\pm 20n \log \left\{ (jwT)^2 + 1 \right\}^{\frac{1}{2}} = \pm 20n \log \sqrt{2} \approx \pm \text{ n } 3\text{db} .$$

The Bode Diagrams of a first order pole and zero at a point on the real axis are given in Fig. (b-5). In Fig. (b-6) the plot of a quadratic zero and pole is shown. Since equation (B-6) is an arithmetical sum of simple terms it is readily seen that any system is easily analysed by the Bode Diagram.

The Bode Diagram offers two convenient parameters for expressing the degree of stability of a feedback system;

Gain margin:

The db gain below 0 db of the loop transfer function at the frequency where the phase shift approaches $\pm\pi$.

Phase margin:

The smaller of the differences between $\pm\pi$ and the phase shift of the loop transfer function where the db gain is zero.

The analysis of the magnetometer is carried out by the method of steady state analysis.

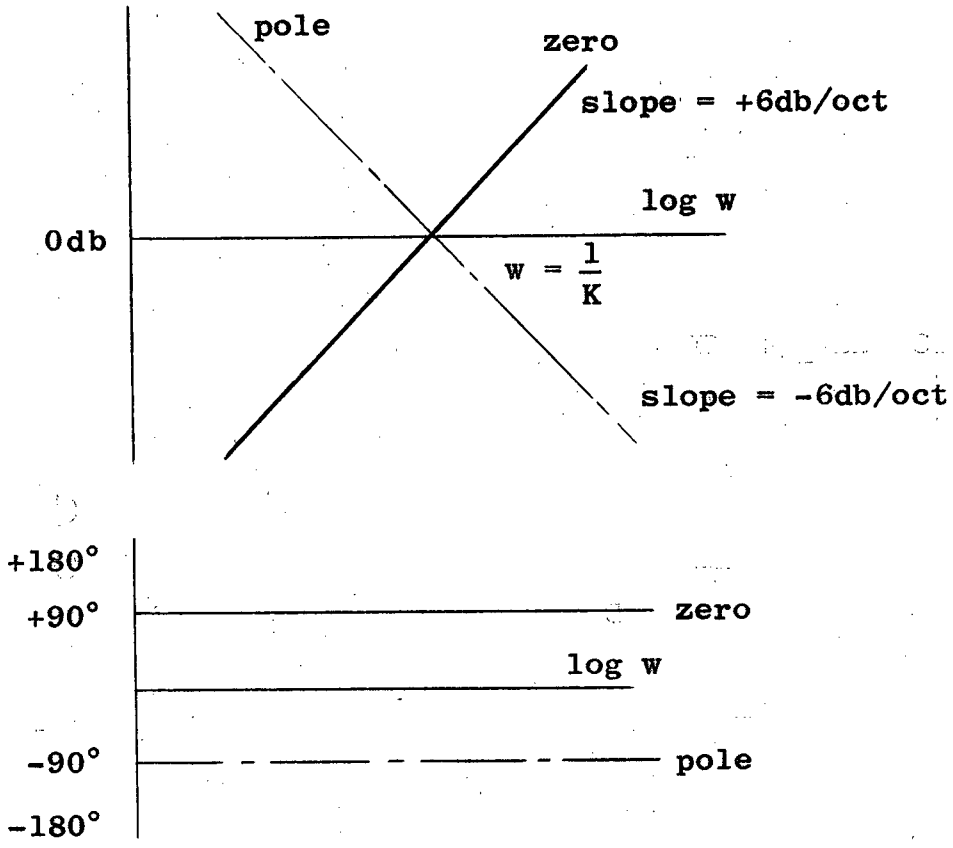

Note: K has been incorporated with $|jw|$.
i.e., $20 \log K|jw| = 0$
when $w = \frac{1}{K}$

Fig. (b-4)

Bode Diagram of First Order Pole and Zero at the Origin.

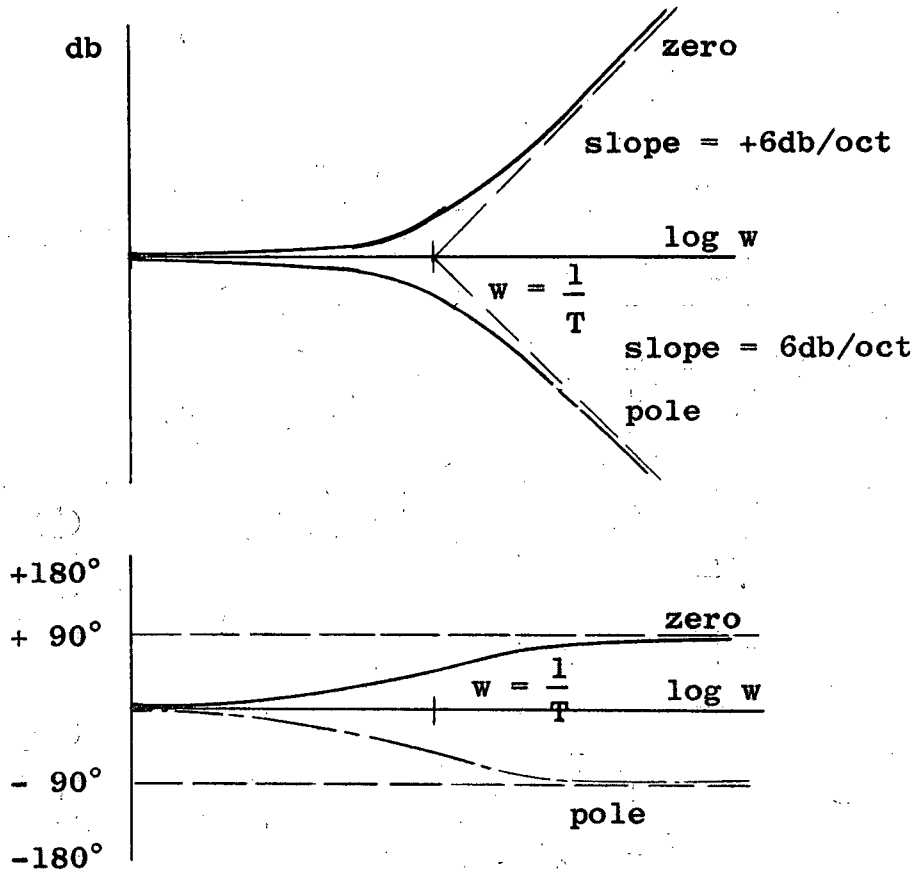

Fig. (b-5)

Bode Diagram of First Order Real Pole and Zero.

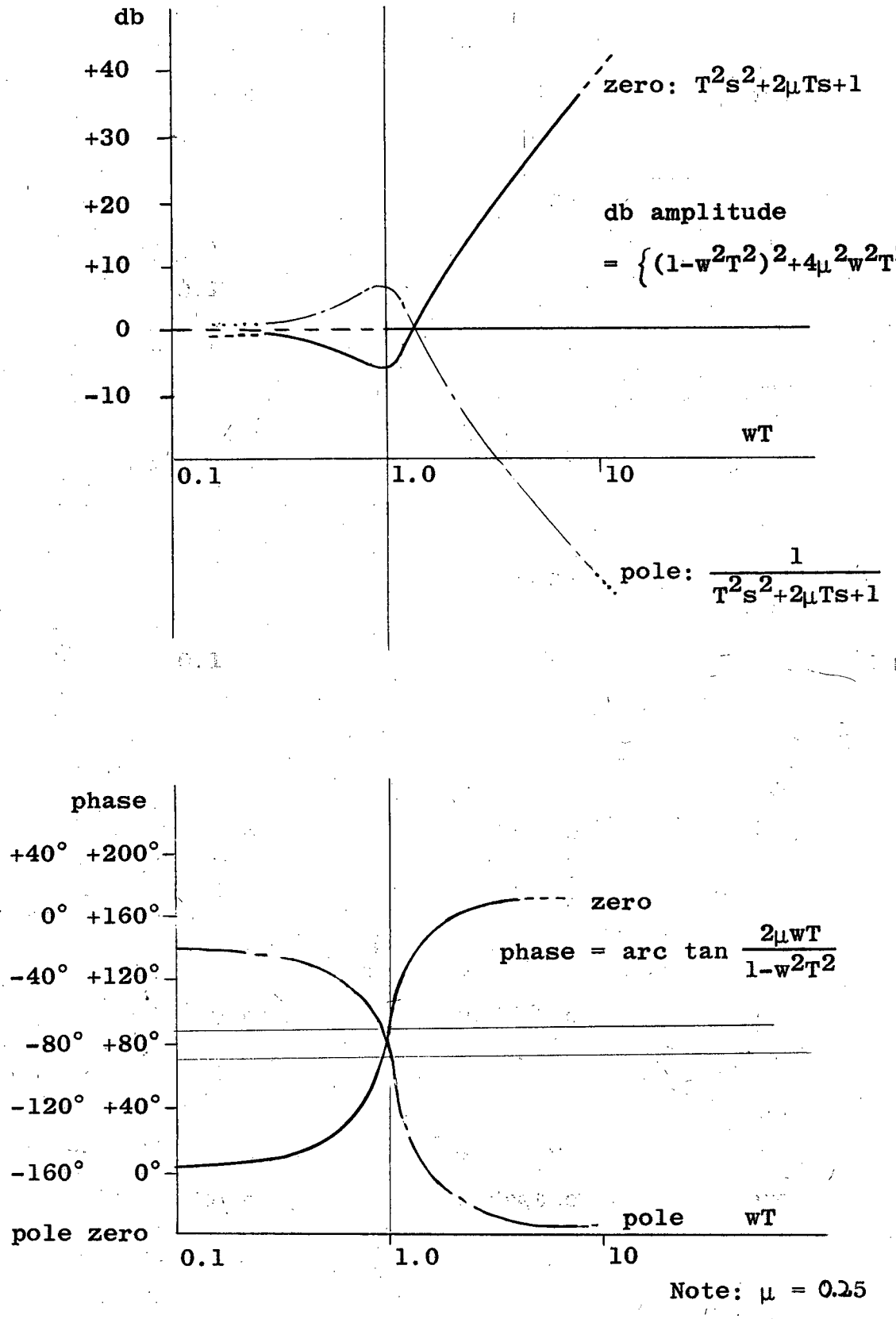

Fig. (b-6)

Bode Diagram of Quadratic Pole and Zero.

BIBLIOGRAPHY

(1) Jacobs, J.A. and K.O. Westphal, 1960, "Geomagnetic Micropulsations", Chemistry and Physics of the Earth, Vol. IV (in press).

(2) Kato, Y. and T. Watanabe, 1958, J. Geophys. Res., 63, 1395-1404.

(3) Toritskaya, V.A., 1953, Dok. Akad. Nauk. SSSR, 91, 241-244.

(4) Serson, P.H., 1957, Can. J. Phys., 35, 1387-1394.

(5) Augenheister, G., 1954, Gerlands Beitr. z. Geophysik, 64, 108-132.

(6) Waters, G.S. and G. Phillips, 1956, Geophys. Prospecting No. 1.

(7) Packard, M. and R. Varian, 1954, Phys. Rev., 93, 941.

(8) Valley, G.E. and H. Wallman, 1948, Vacuum Tube Amplifiers, M.I.T. Radiation Laboratory Series, 18, 490.

(9) Whittles, A.B.L., 1960, M.Sc. Thesis, University of British Columbia.

(10) Maxwell, A., 1957, International Geophysical Year Annals, 4, 281-286.

(11) Sinno, K., 1960, Private Communication.

(12) Bloch, F., 1946, Phys. Rev., 70, 460-474.

(13) Bloch, F. and W. Hansen and M. Packard, 1946, Phys. Rev., 70, 474-485.

(14) Bloch, F. and A. Siegert, 1940, Phys. Rev., 57, 522.

(15) Bloch, F., 1946, Phys. Rev., 70, 460-474.

(16) Ahrendt, W. and C. Savant, Jr., Servomechanism Practice, 132.

(17) Valley, G.E. and H. Wallman, Vacuum Tube Amplifiers, M.I.T. Radiation Laboratory Series, 18, 441-458.

(18) Jones, E.P., 1959, M.Sc. Thesis, University of British Columbia.

(19) Cheng, D.K., Analysis of Linear Systems, 398-402.

(20) Bateman Manuscript Project, Tables of Integral Transforms, 1, 129-299.

(21) Langevin, P., 1905, J. Phys. théor. appl., (4), 4, 678.

(22) Bloch, F., 1946, Phys. Rev., 70, 460-474.

(23) Andrew, E., 1955, Nuclear Magnetic Resonance, 221-223.

(24) Bloch, F., 1946, Phys. Rev., 70, 462.

GENERAL REFERENCES

Nuclear Magnetic Resonance

Andrew, .R., 1955, Nuclear Magnetic Resonance.

Bloembergen, N., 1948, Nuclear Magnetic Relaxation.

Pake, G.E., 1950, Am. J. Phys., 18, 438-452, 473-486.

Roberts, J.D., 1959, Nuclear Magnetic Resonance.

Saha, A. and T. Das, 1956, Theory and Applications of Nuclear Induction.

Feedback System Analysis

Ahrendt, W. and C.J. Savant, Jr., 1960, Servomechanism Practice.

Angelo, E.J., Jr., 1958, Electronic Circuits.

Aseltine, J.A., 1958, Transform Method in Linear System Analysis.

Chance, B. et al., 1948, Waveforms, M.I.T. Radiation Laboratory Series, Vol. 19.

Cheng, D.K., 1959, Analysis of Linear Systems.

Fich, S., 1959, Transient Analysis in Electrical Engineering.

Greenwood, I. et al., 1946, Electronic Instruments, M.I.T. Radiation Laboratory Series, Vol. 21.

James, H. et al., 1947, Theory of Servomechanisms, M.I.T. Radiation Laboratory Series, Vol. 25.

Landee, R.W. et al., 1957, Electronic Designers Handbook.

Laning, J. and R. Battin, 1956, Random Processes in Automatic. Control.

Murphy, G.J., 1957, Basic Automatic Control Theory.

Savant, C.J., Jr., 1958, Basic Feedback Control System Design.

Valley, G.E. and H. Wallman, 1948, Vacuum Tube Amplifiers, M.I.T. Radiation Laboratory Series, Vol. 18.

Others

Bleaney, B.I. and B. Bleaney, 1957, Electricity and Magnetism.

Chapman, S. and J. Bartels, 1951, Geomagnetism, Vol. 1 and 2.

Nagaoka, H., 1921, Phil. Mag., 6-41, 377-388.